Electronic Supplementary Information for:

Synthesis, structural studies, and redox chemistry of bimetallic [Mn(CO)$_3$] and [Re(CO)$_3$] complexes

Wade C. Henke,[a] Tyler A. Kerr,[a] Thomas R. Sheridan,[b] Lawrence M. Henling,[b] Michael K. Takase,[b] Victor W. Day,[a] Harry B. Gray,[b] and James D. Blakemore[a,b]*

[a] Department of Chemistry, University of Kansas
1567 Irving Hill Road, Lawrence, KS 66045

[b] Beckman Institute and Division of Chemistry and Chemical Engineering,
California Institute of Technology, Pasadena, California 91125

* To whom correspondence should be addressed.
e-mail: blakemore@ku.edu; phone: +1 (785) 864-3019

Contents

NMR Spectra

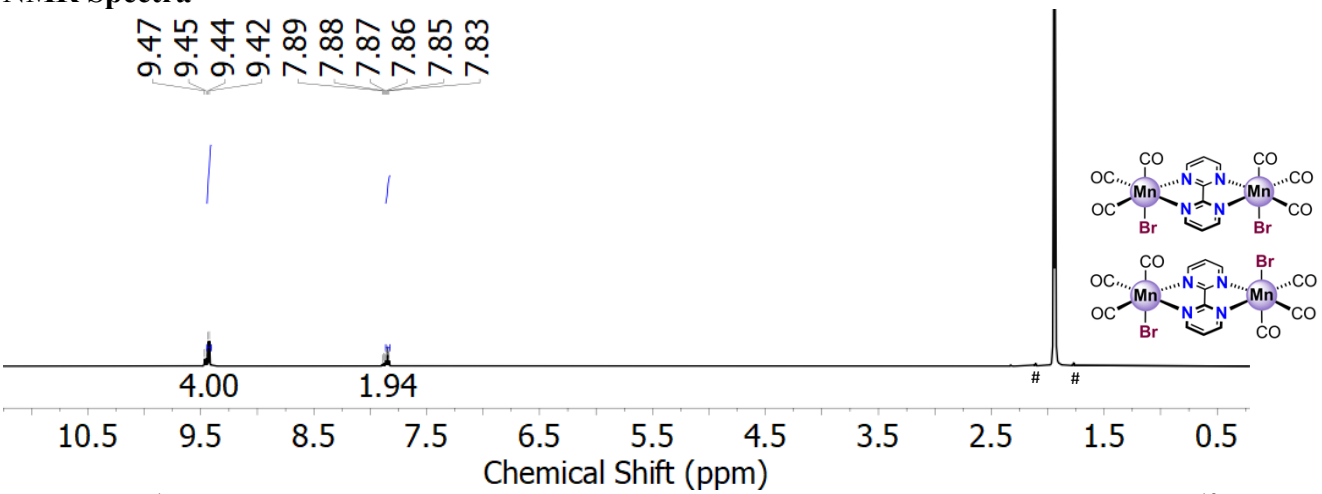

Figure S1: ^{1}H-NMR spectrum (400 MHz, CD_3CN) of **5-syn** + **5-anti**. The # symbols denote ^{13}C satellites on the CD_3CN protio-solvent residual.

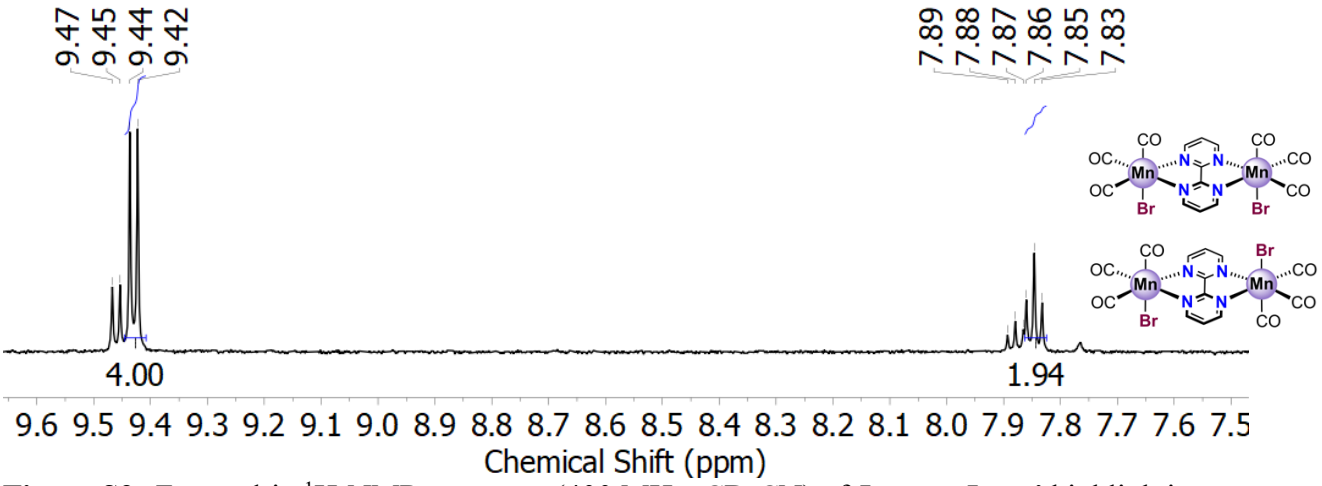

Figure S2: Zoomed-in ^{1}H-NMR spectrum (400 MHz, CD_3CN) of **5-syn** + **5-anti** highlighting the aromatic region.

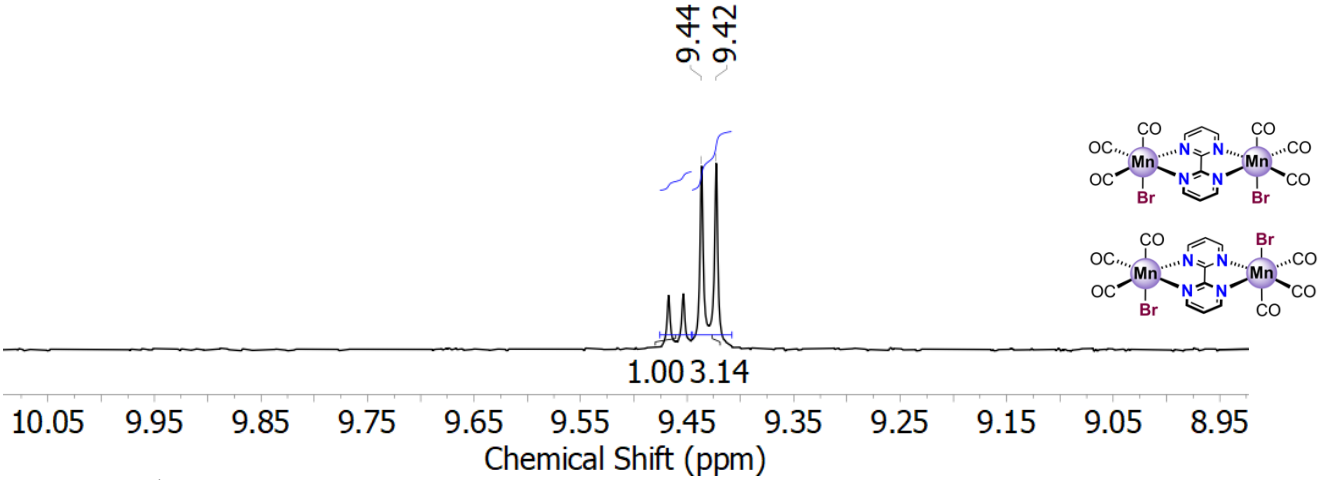

Figure S3: ^{1}H-NMR spectrum (400 MHz, CD_3CN) comparing the ratio of **5-syn** + **5-anti**.

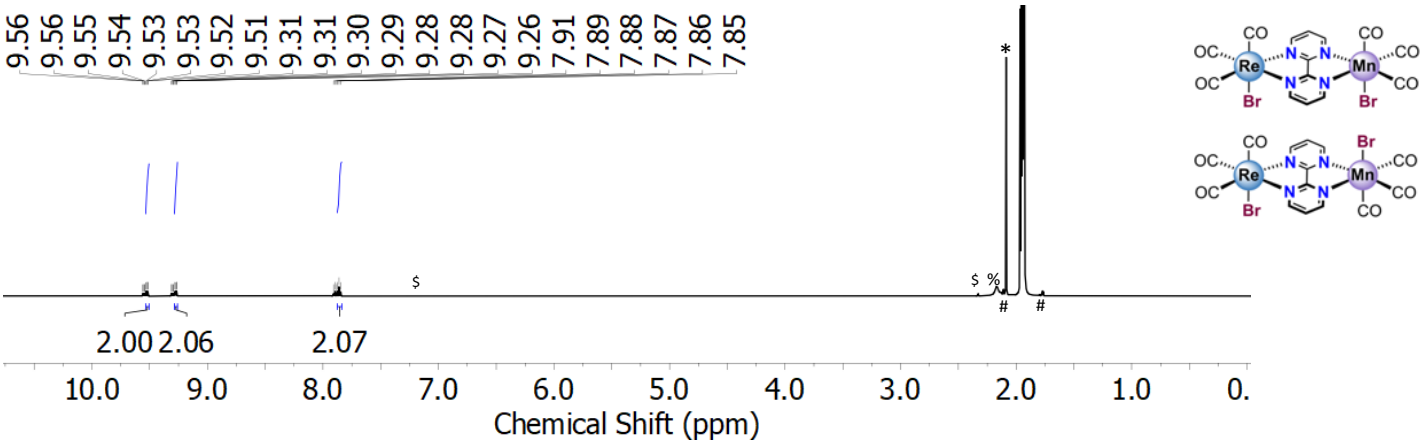

Figure S4: ^{1}H-NMR spectrum (400 MHz, CD_3CN) of **6-syn** + **6-anti**. The symbols denote the ^{13}C satellites on the CD_3CN protio-solvent residuals (#), toluene ($), water (%), and adventitious acetone (*).

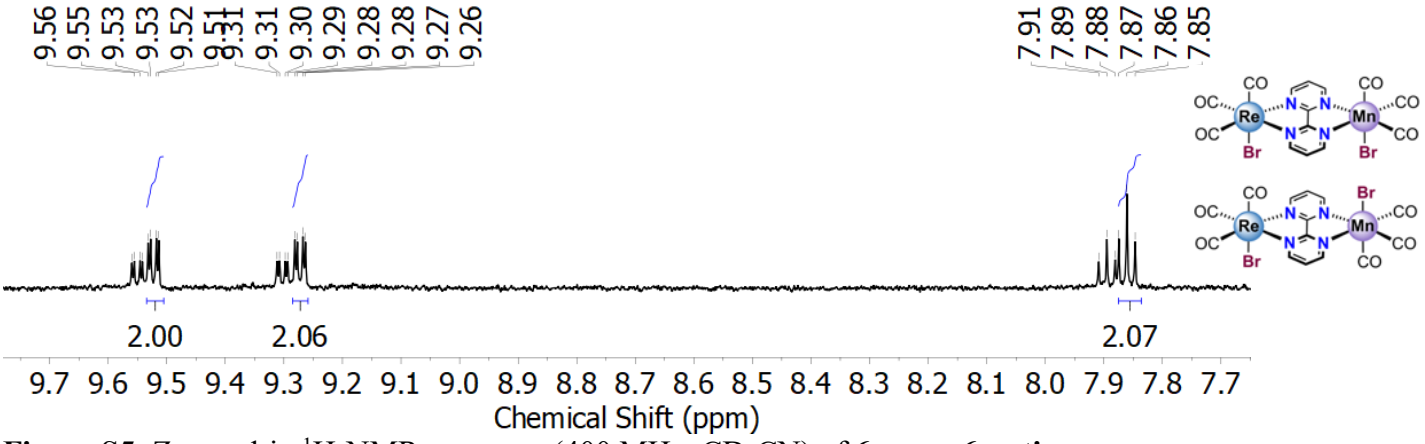

Figure S5: Zoomed-in ^{1}H-NMR spectrum (400 MHz, CD_3CN) of **6-syn** + **6-anti**

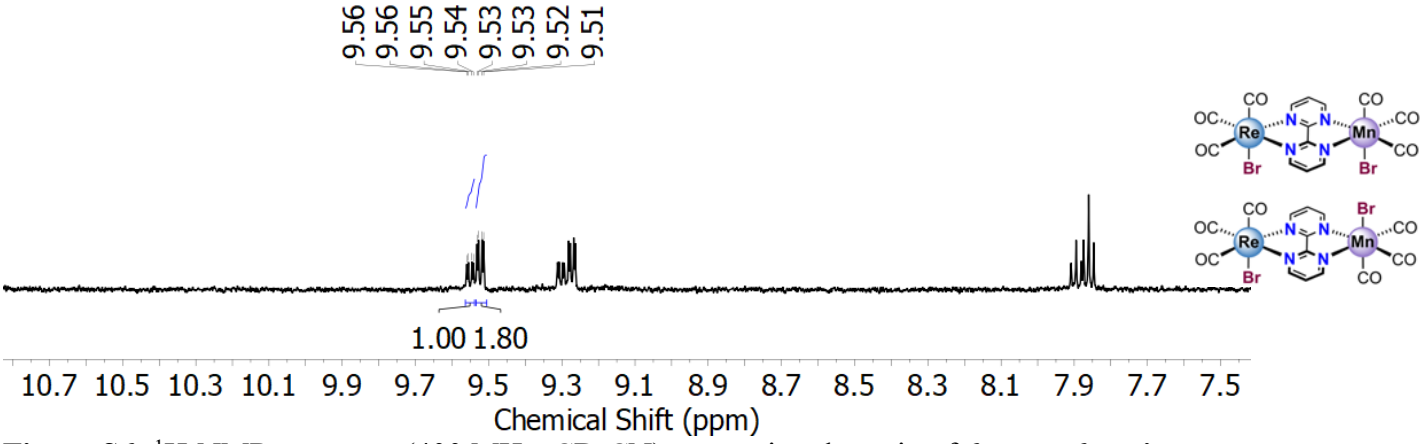

Figure S6: ^{1}H-NMR spectrum (400 MHz, CD_3CN) comparing the ratio of **6-syn** + **6-anti**.

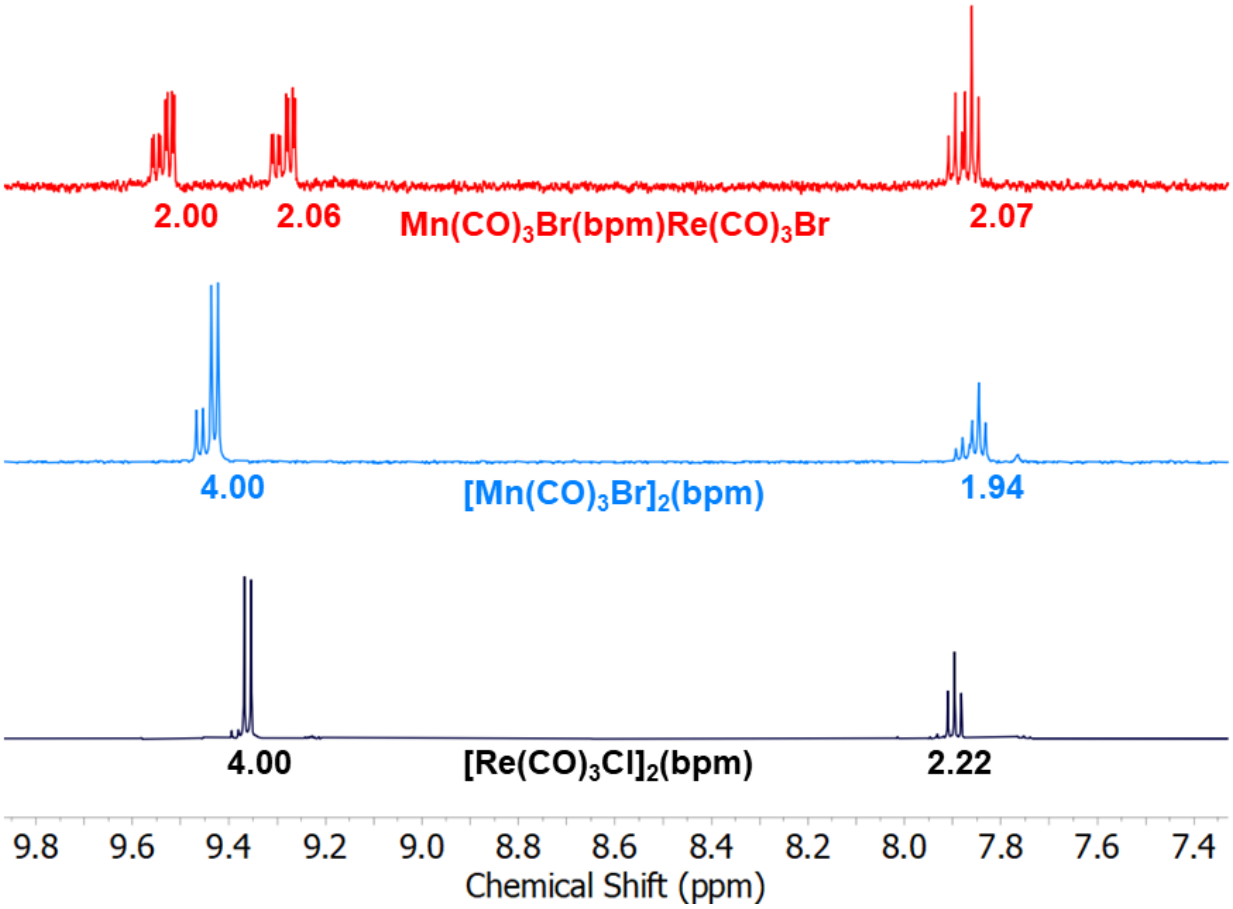

Figure S7: Stacked ^{1}H-NMR spectra (400 MHz, CD_3CN) of **2-syn + 2-anti (black), 5-syn + 5-anti (blue), and 6-syn + 6-anti (red)**. The presence of both **syn-** and **anti**-isomers give rise to the additional resonances in the spectra.

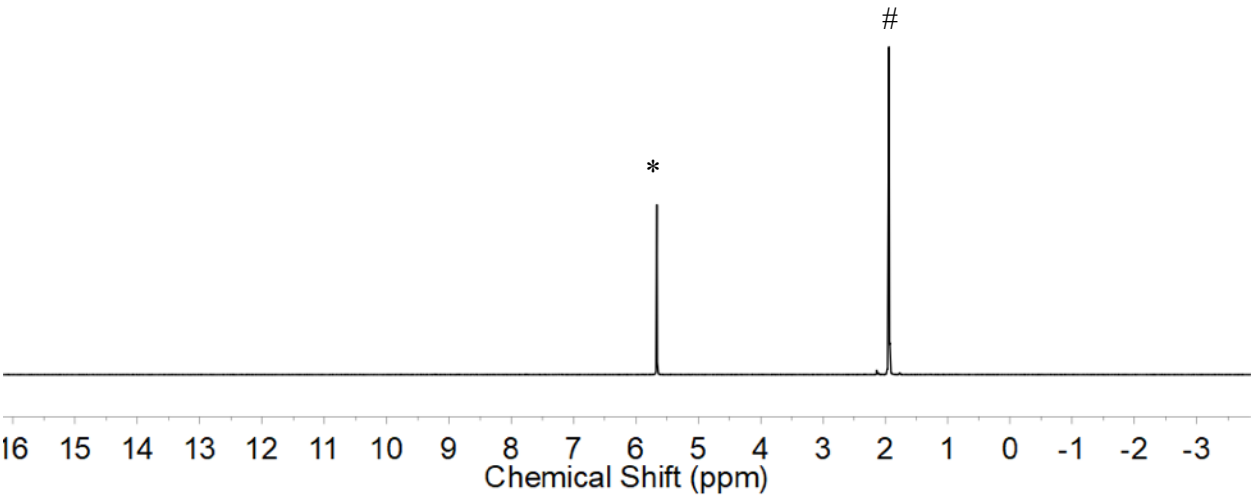

Figure S8: The resulting ^{1}H-NMR spectrum (400 MHz, CD_3CN) following the *in situ* one e^- reduction of complex **2-syn + 2-anti** using the stoichiometric reductant Cp_2Co. The resulting complex is NMR silent, consistent with the presence of an expected paramagnetic species. The presence of $[Cp_2Co]Cl$ (*, 5.66 ppm) and the solvent residual $CD_2(H)CN$ (#).

IR Spectra

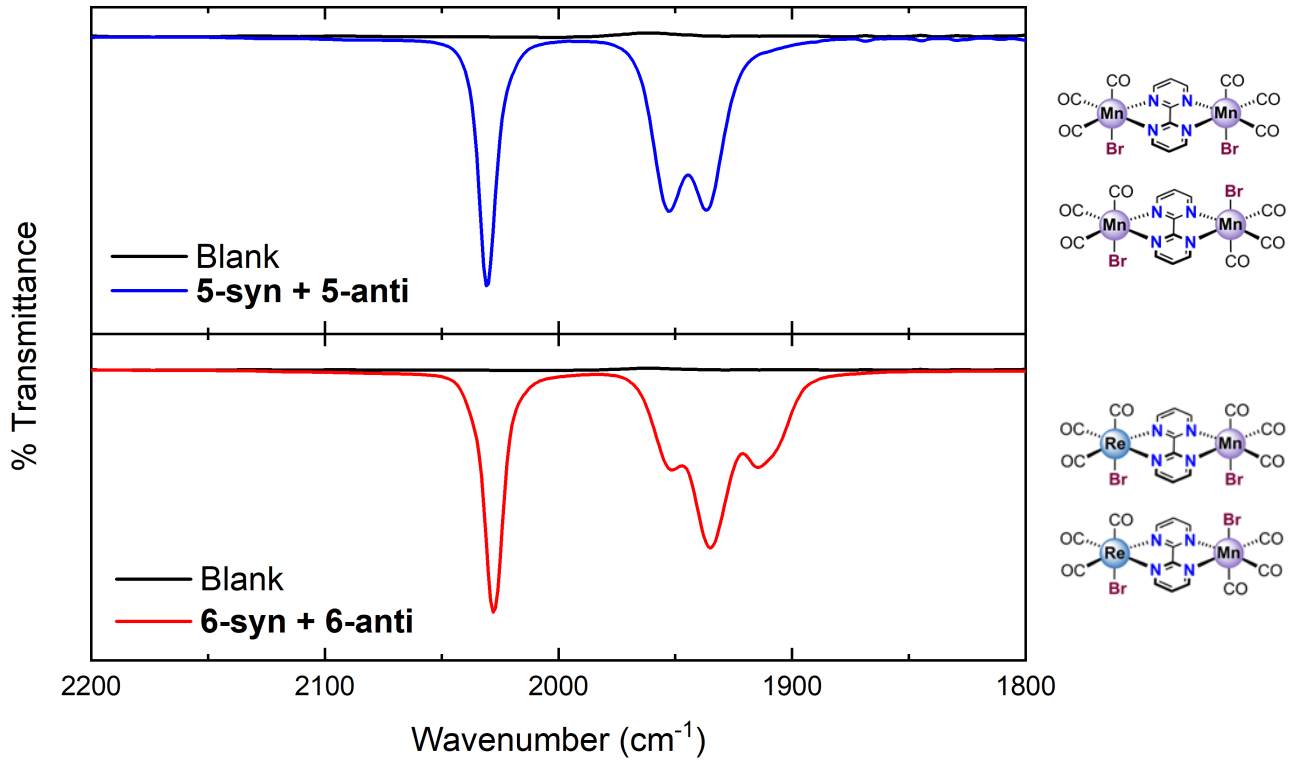

Figure S9: IR spectra for the CO stretching region showing the carbonyl stretches for **5-syn** + **5-anti** (upper panel) and **6-syn** + **6-anti** (lower panel) in THF solution. The greater number of CO stretches for **6-syn** + **6-anti** in comparison to **5-syn** + **5-anti** can be attributed to the lower symmetry of the heterobimetallic compound. The symmetries of **5-syn** + **5-anti** are C_{2v} and C_{2h}, respectively. Group theory analysis predicts that **5-syn** should have six IR active bands while **5-anti** should have three IR active bands. Experimentally, there is likely significant overlap of bands for the CO stretches, as they should have very similar energies, resulting in only three apparent bands. The symmetries of **6-syn** + **6-anti** are both C_s. Group theory analysis thus predicts that both compounds should each have six IR-active CO stretching modes. Experimentally, the observation of a greater number of overlapping bands is consistent with the decreased symmetry as well as the anticipated electronic difference between the $[Mn(CO)_3]$ and $[Re(CO)_3]$ motifs in both isomers.

High Resolution Mass Spectra

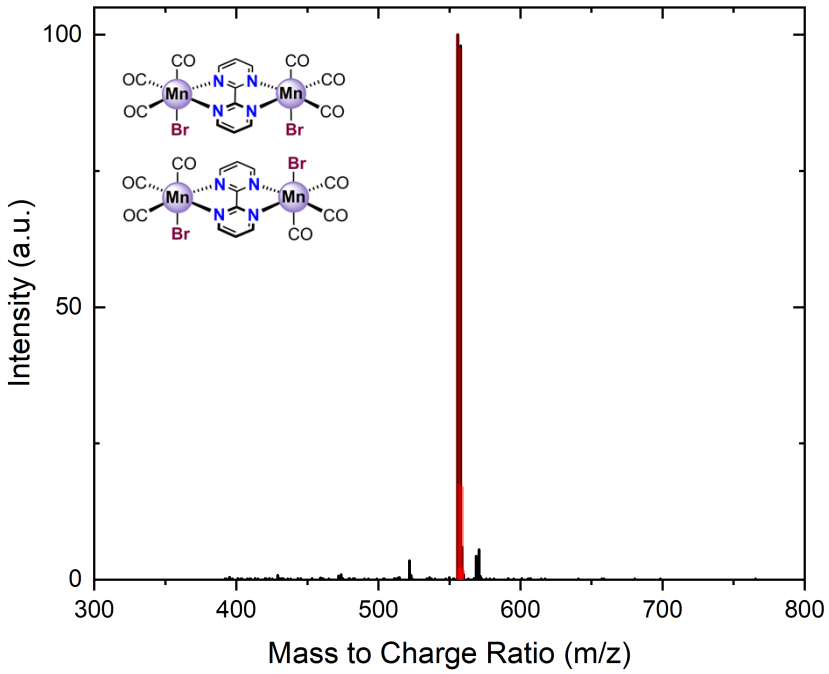

Figure S10: Full high-resolution mass spectrum of **5-syn** + **5-anti**. Both syn and anti isomers could be present and the resulting acetonitrile ligand could bind to either Re or Mn. The experimental data is shown in **black** and the predicted data is shown in **red**. The identified fragment is given in detail below.

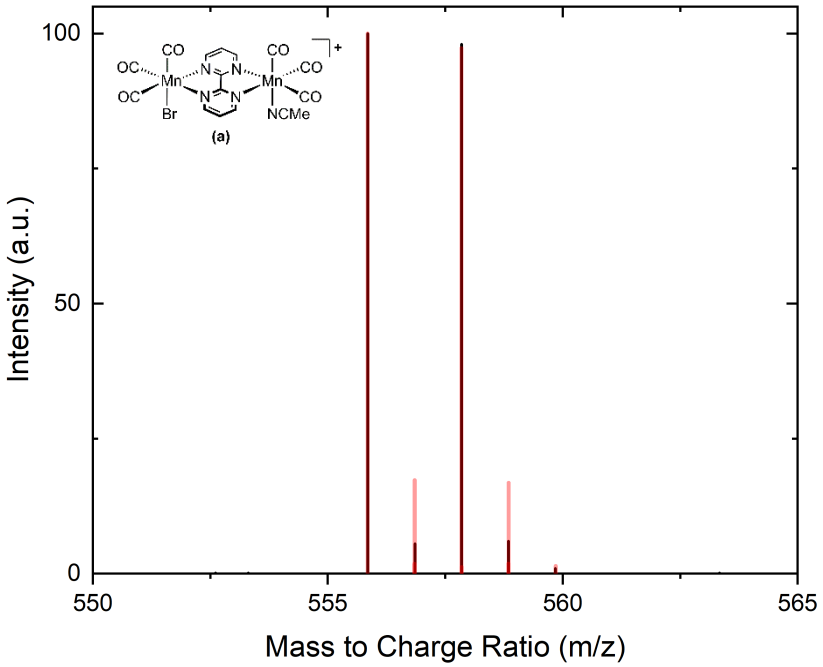

Figure S11: Fragment **(a)** was the identified fragement in the data from Figure S10 (**Experimental: 555.8495; Theoretical: 555.8497**).

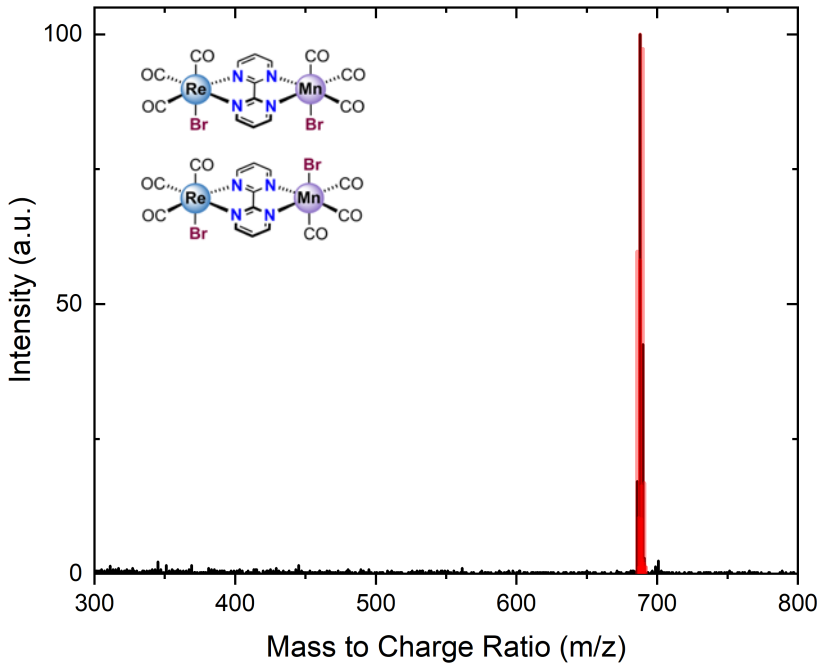

Figure S12: Full high-resolution mass spectrum of **6-syn** + **6-anti**. Both syn and anti isomers could be present, and the resulting acetonitrile ligand could bind to Re or Mn. The experimental data is shown in **black** and the predicted data is shown in **red**. The identified fragment is investigated below.

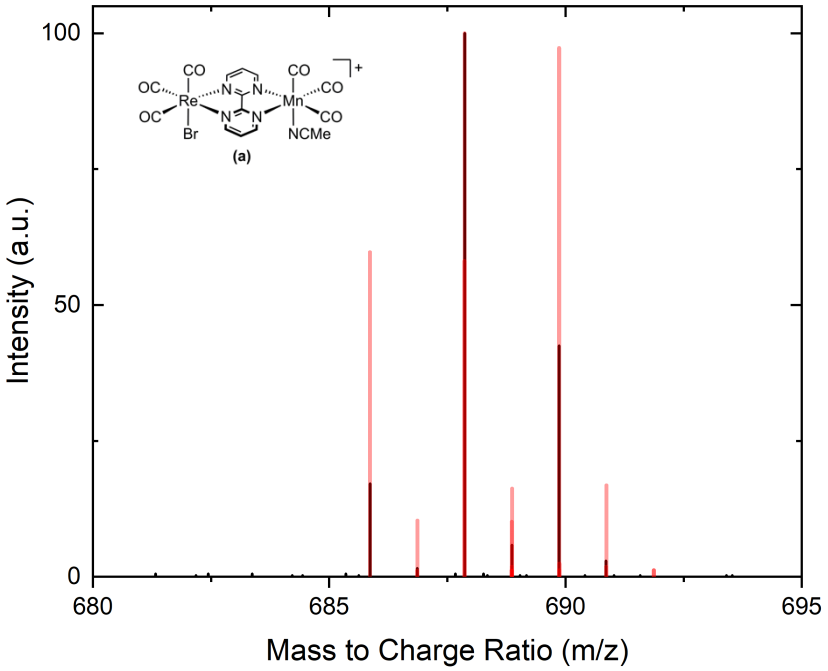

Figure S13: Fragment **(a)** was the identified fragment in the data from Figure S12 (**Experimental: 687.8672; Theoretical: 687.8674**).

Electronic Absorption Spectra

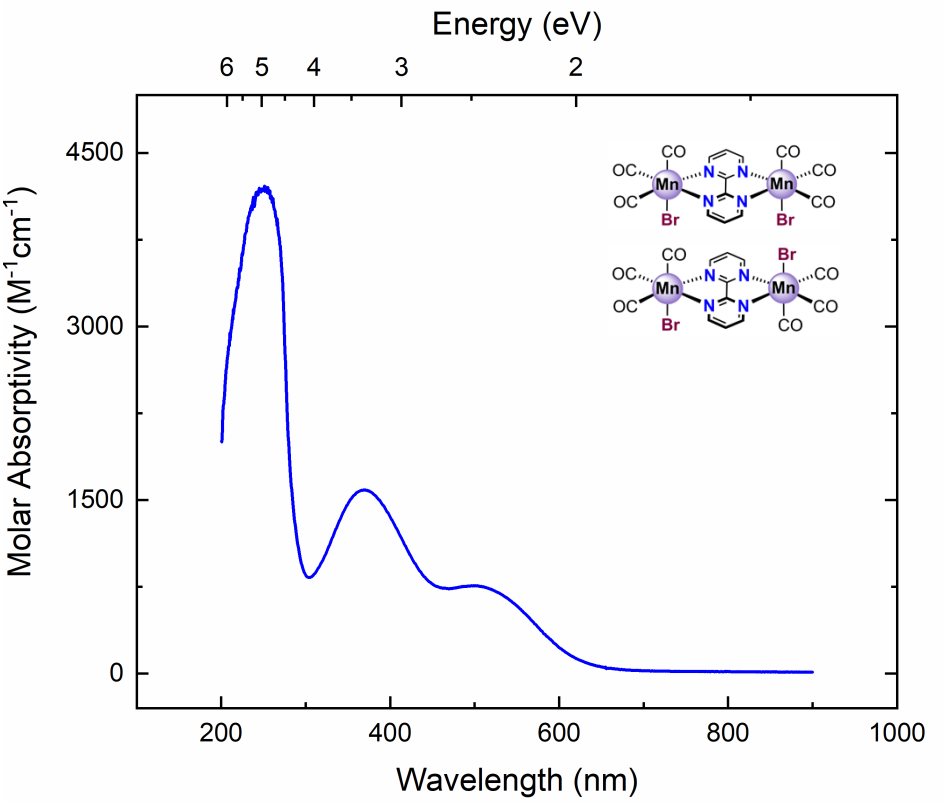

Figure S14: Electronic absorption spectrum of **5-syn** + **5-anti** in MeCN.

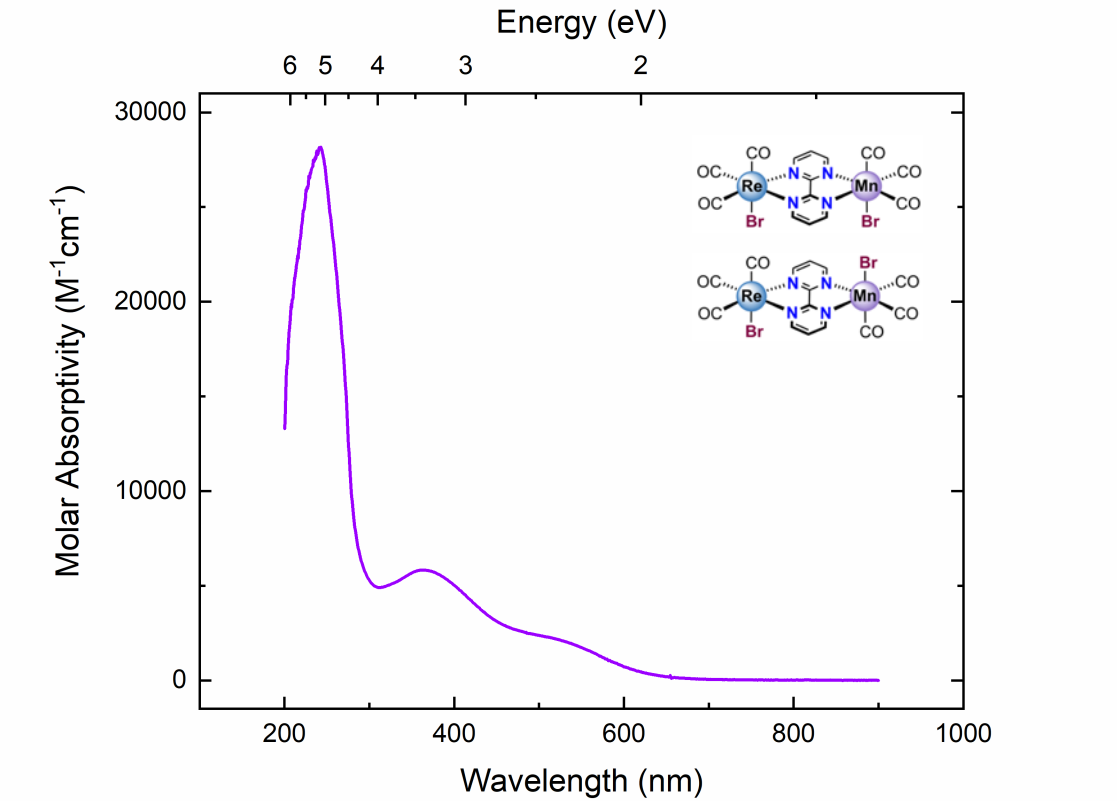

Figure S15: Electronic absorption spectrum of **6-syn** + **6-anti** in MeCN.

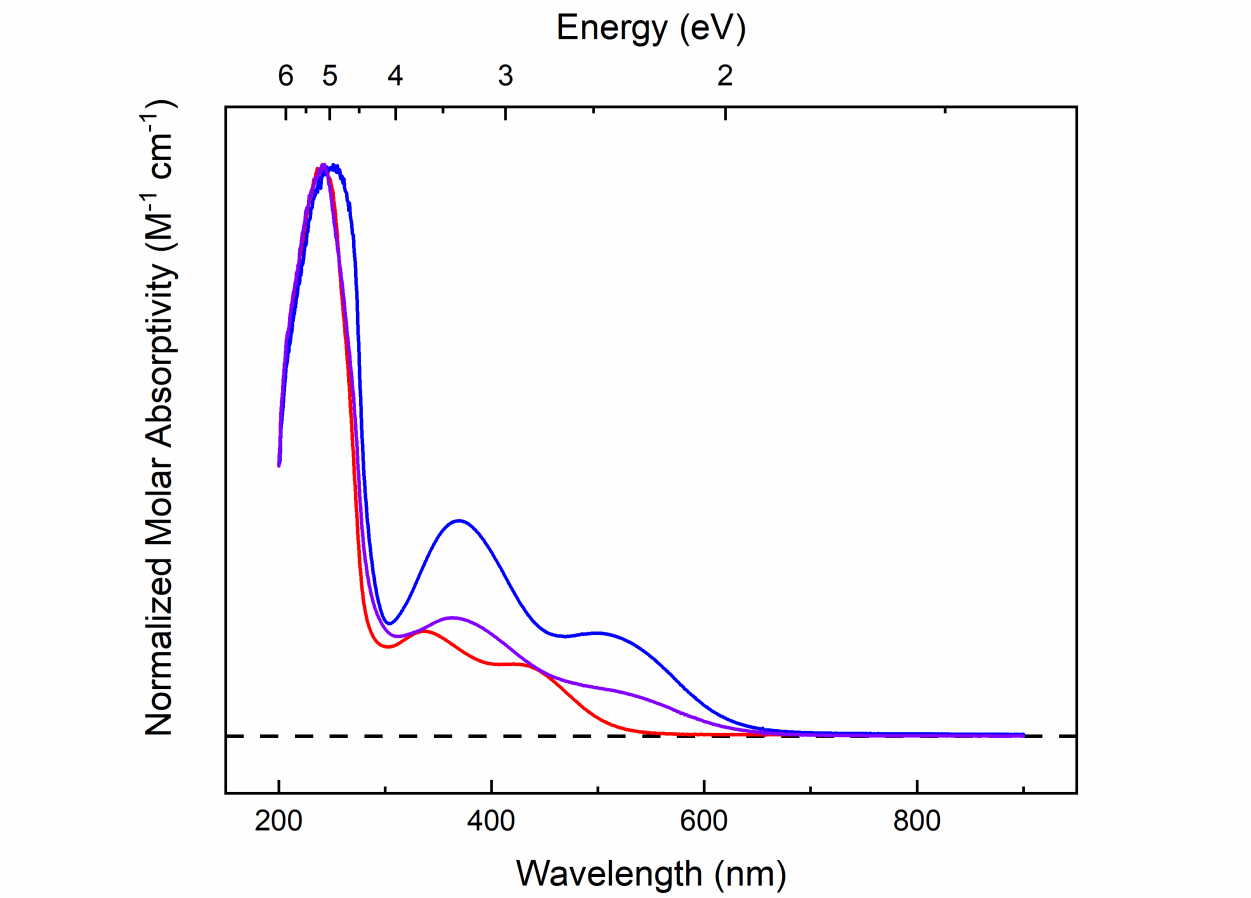

Figure S16: Normalized stacked electronic absorption spectra of **4 (red)**, **5-syn + 5-anti (blue),** and **6-syn + 6-anti (purple)** in MeCN.

Cyclic Voltammetry Data

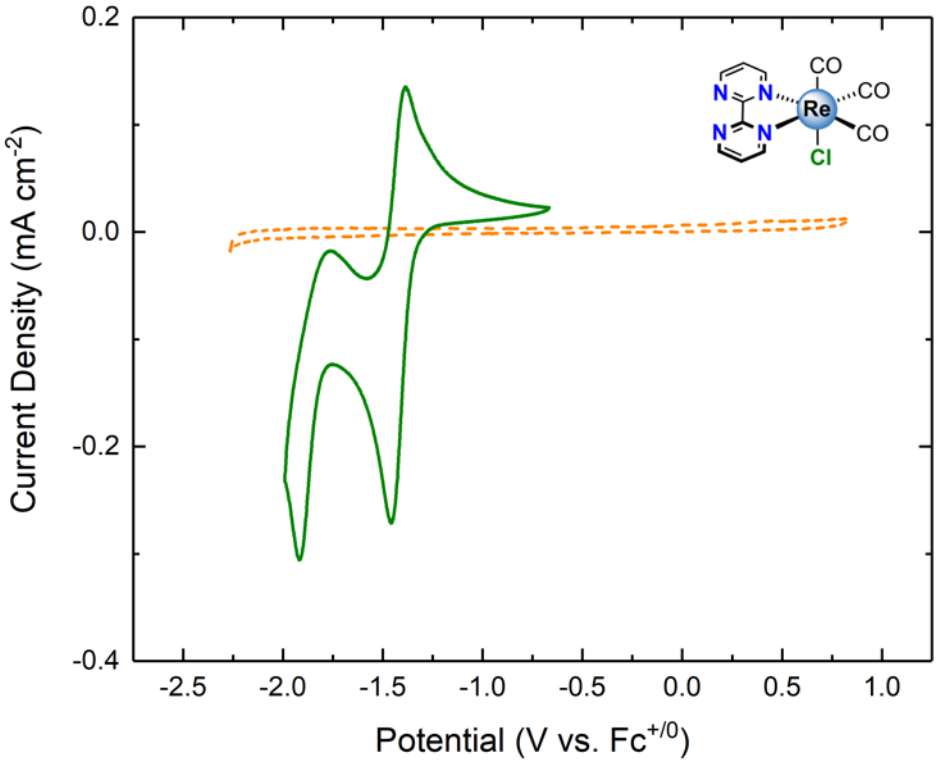

Figure S17: Cyclic voltammogram (100 mV/s) of **1** (**green**) in 0.1M $TBAPF_6$/MeCN solution. The **orange** trace is the blank taken prior to beginning the experiment.

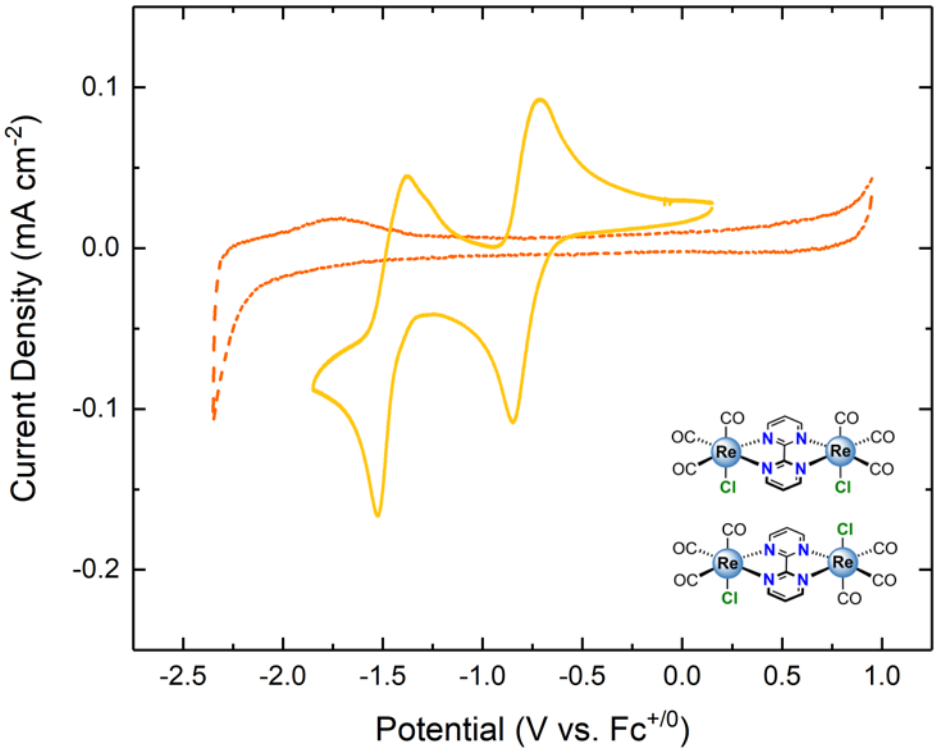

Figure S18: Cyclic voltammogram (100 mV/s) of **2-syn + 2-anti** (**yellow**) in 0.1M $TBAPF_6$/MeCN solution. The **orange** trace is the blank taken prior to beginning the experiment.

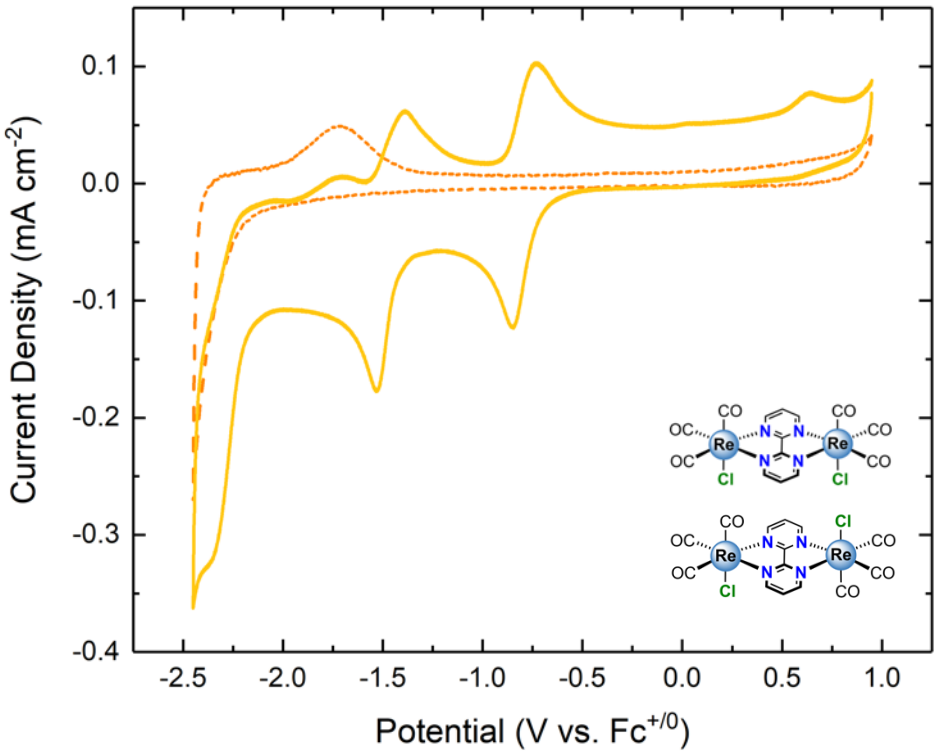

Figure S19: Extended cyclic voltammogram (100 mV/s) of **2-syn** + **2-anti** (**yellow**) in 0.1M $TBAPF_6$/MeCN solution. The **orange** trace is the blank taken prior to beginning the experiment.

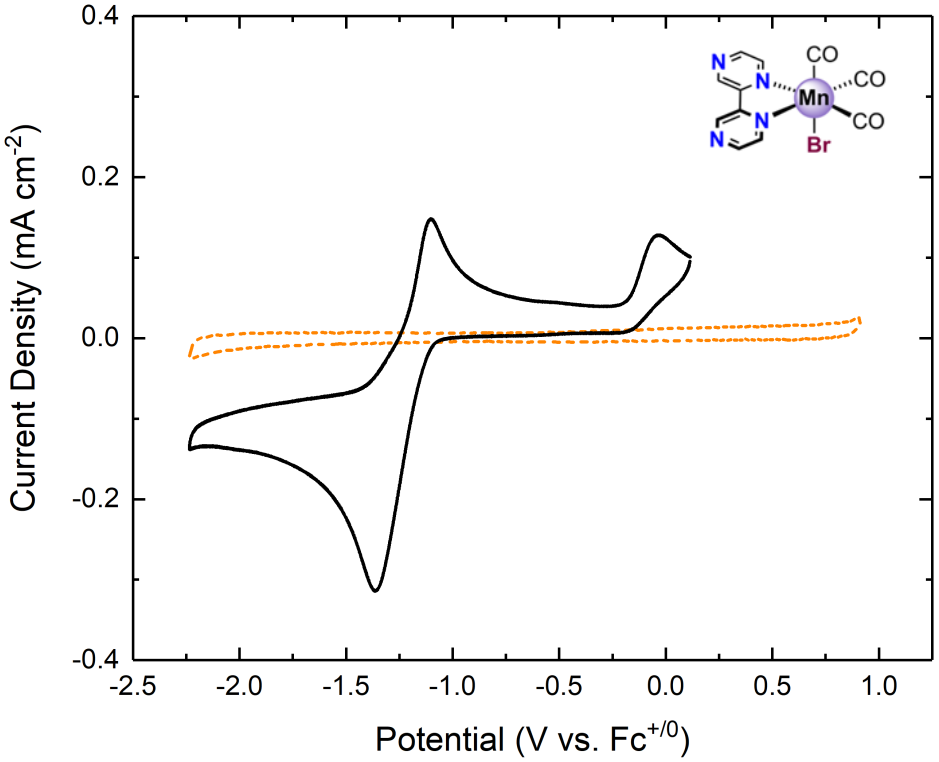

Figure S20: Cyclic voltammogram (100 mV/s) of **3** (**black**) in 0.1M $TBAPF_6$/MeCN solution. The **orange** trace is the blank taken prior to beginning the experiment.

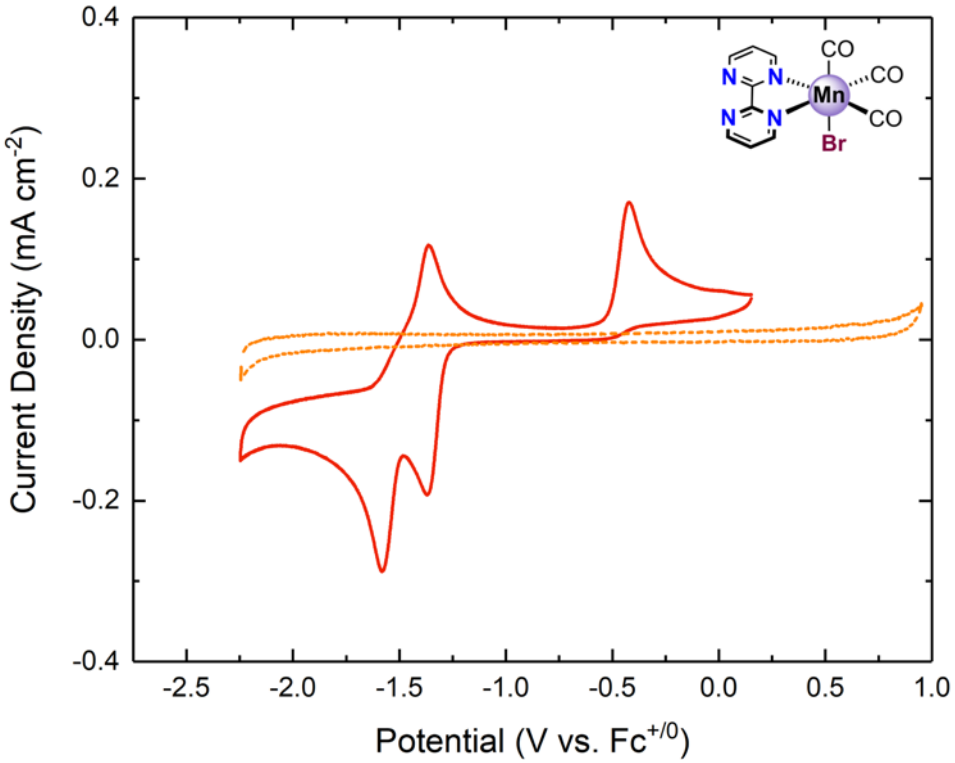

Figure 21: Cyclic voltammogram (100 mV/s) of **4** (**red**) in 0.1M $TBAPF_6$/MeCN solution. The **orange** trace is the blank taken prior to beginning the experiment.

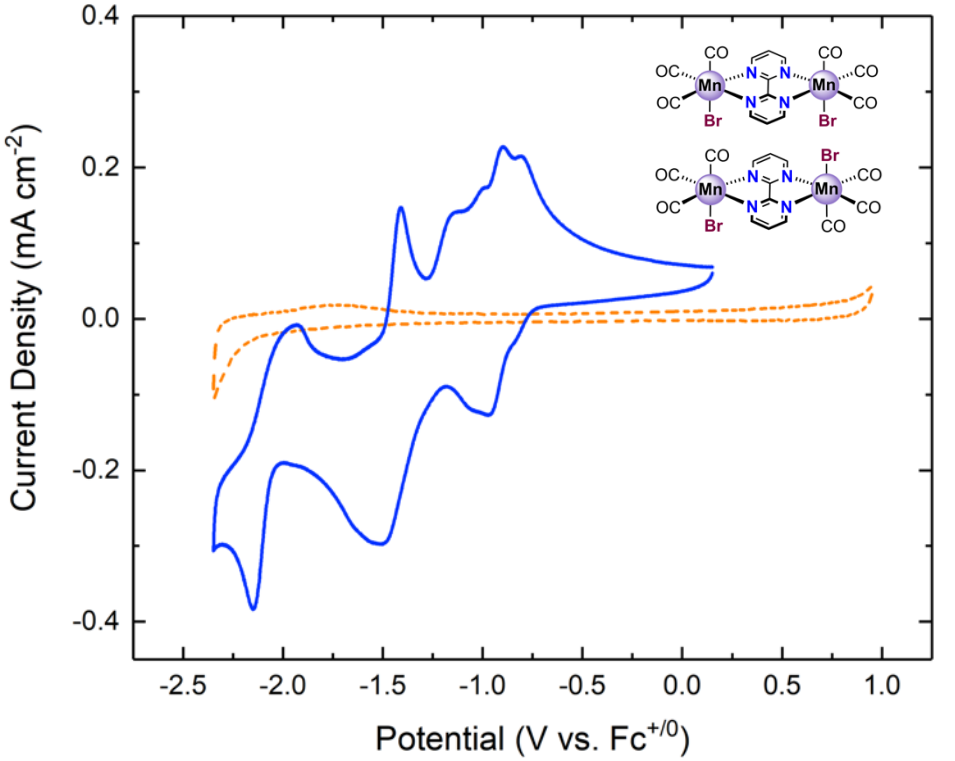

Figure S22: Cyclic voltammogram (100 mV/s) of **5-syn** + **5-anti** (**blue**) in 0.1M $TBAPF_6$/MeCN solution. The **orange** trace is the blank taken prior to beginning the experiment.

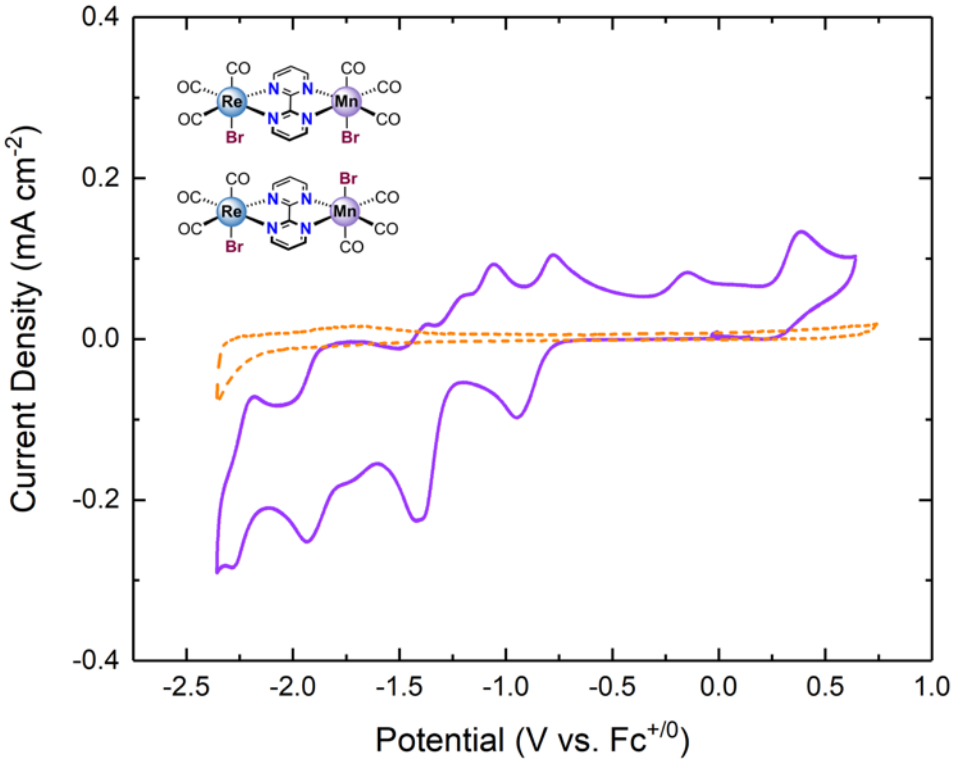

Figure S23: Cyclic voltammogram (100 mV/s) of **6-syn + 6-anti** (**purple**) in 0.1M $TBAPF_6$/MeCN solution. The **orange** trace is the blank taken prior to beginning the experiment.

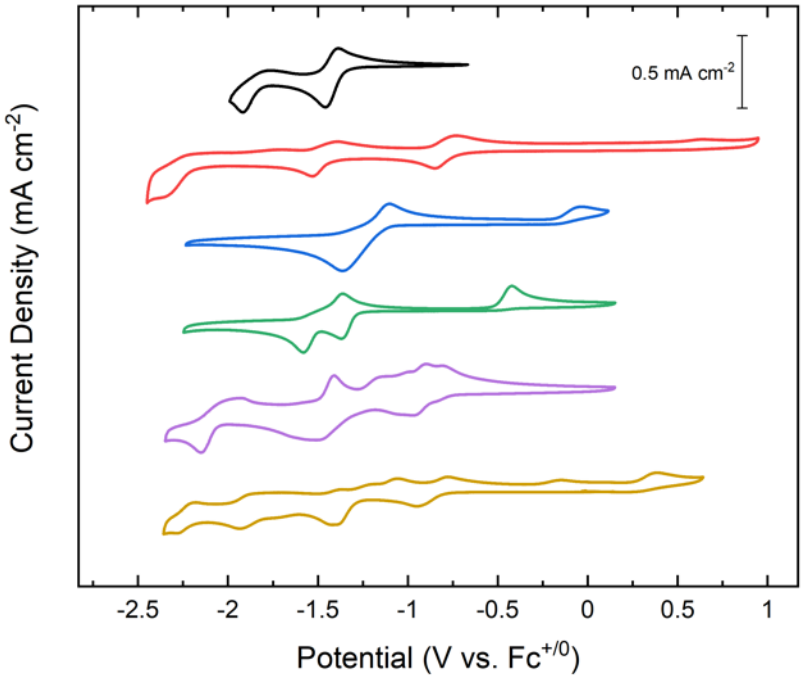

Figure S24: Stacked cyclic voltammograms (100 mV/s) of complexes **1-6** in 0.1M $TBAPF_6$/MeCN solution. **1** (**black**), **2-syn** + **2-anti** (**red**), **3** (**blue**), **4** (**green**), **5-syn** + **5-anti** (**purple**), **6-syn + 6-anti** (**gold**).

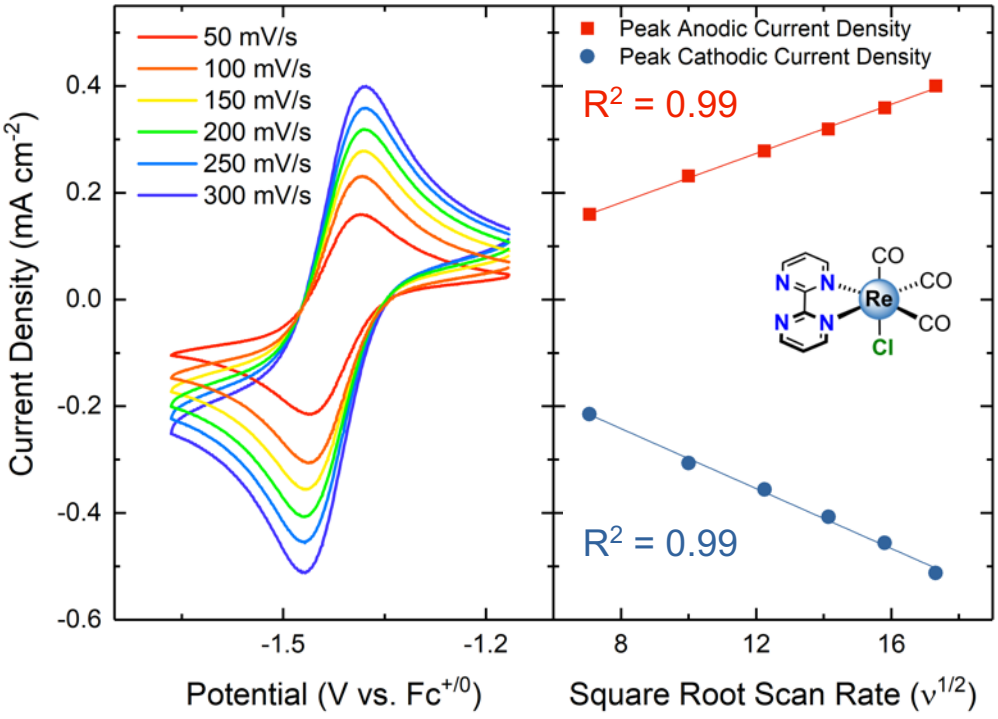

Figure S25: Scan rate dependence studies (left) and peak anodic and cathodic current density as a function of the square root of scan rate (right) for the first redox couple of complex **1**.

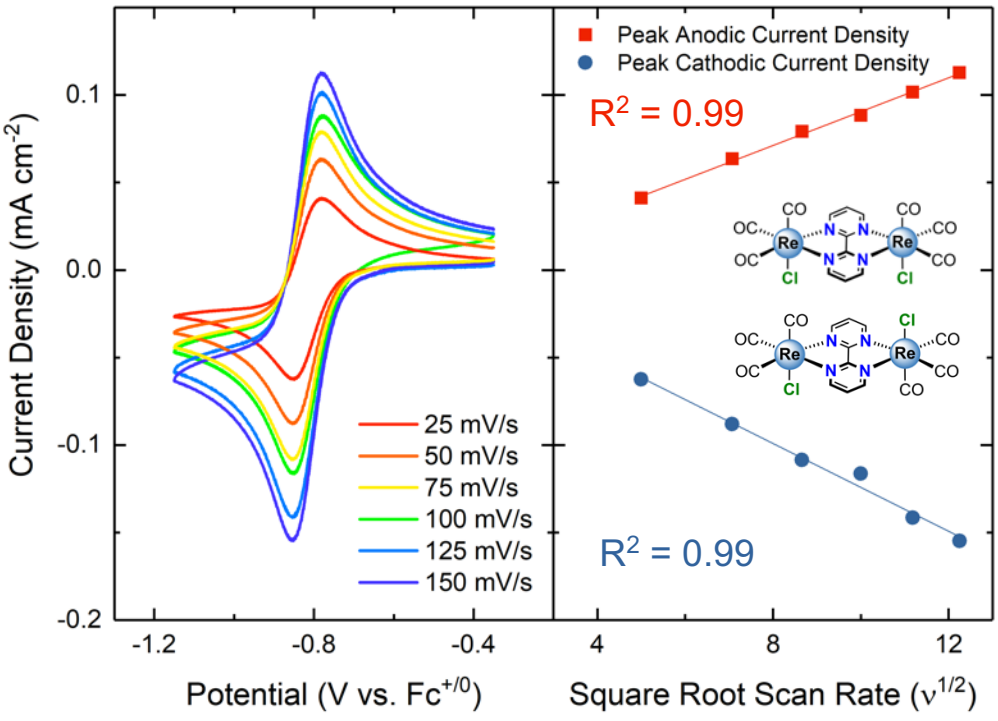

Figure S26: Scan rate dependence studies (left) and peak anodic and cathodic current density as a function of the square root of scan rate (right) for the first redox couple of complex **2-syn** + **2-anti**.

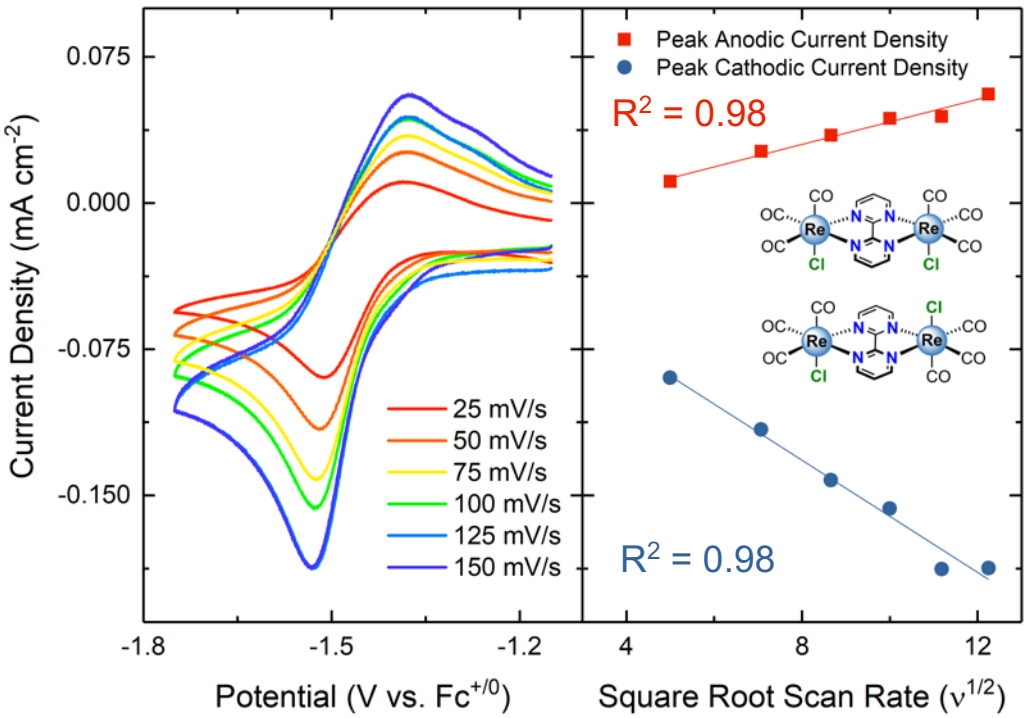

Figure S27: Scan rate dependence studies (left) and peak anodic and cathodic current density as a function of the square root of scan rate (right) for the second redox couple of complex **2-syn** + **2-anti**.

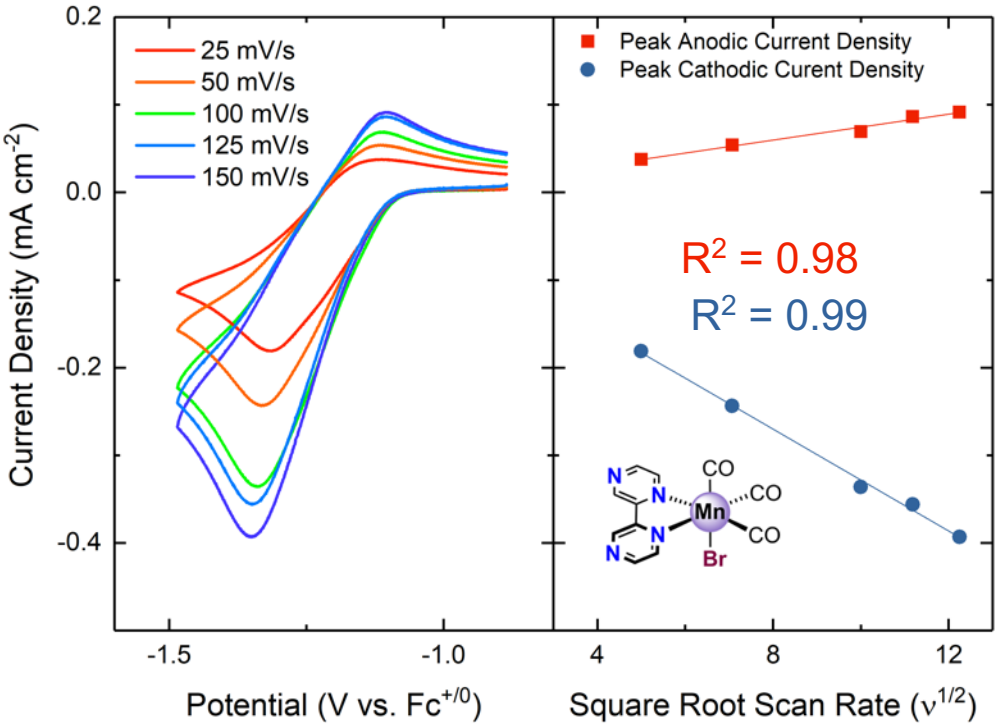

Figure S28: Scan rate dependence studies (left) and peak anodic and cathodic current density as a function of the square root of scan rate (right) for complex **3**.

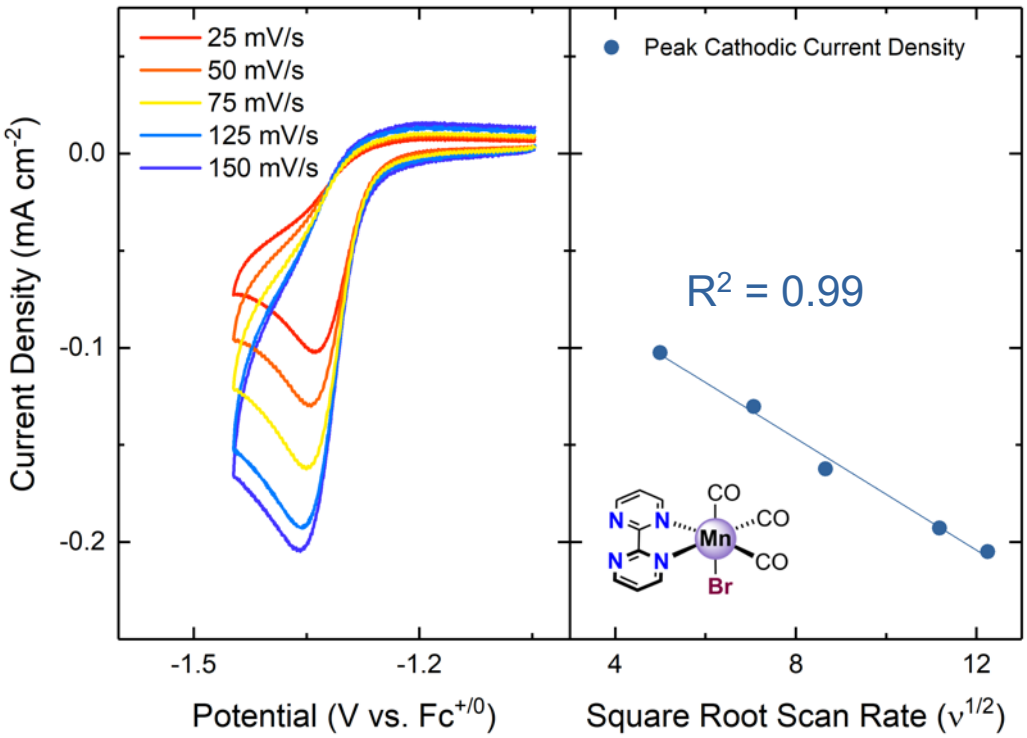

Figure S29: Scan rate dependence studies (left) and peak anodic and cathodic current density as a function of the square root of scan rate (right) for complex **4**.

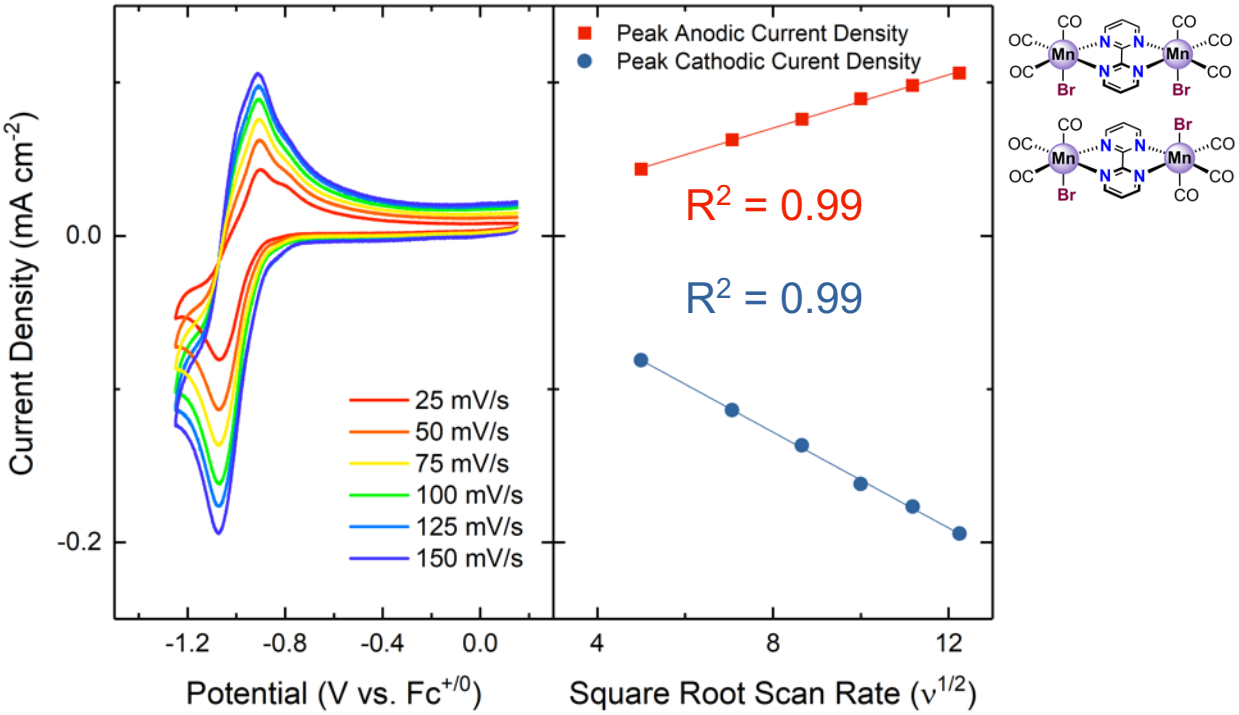

Figure S30: Scan rate dependence studies (left) and peak anodic and cathodic current density as a function of the square root of scan rate (right) for complex **5-syn** + **5-anti**.

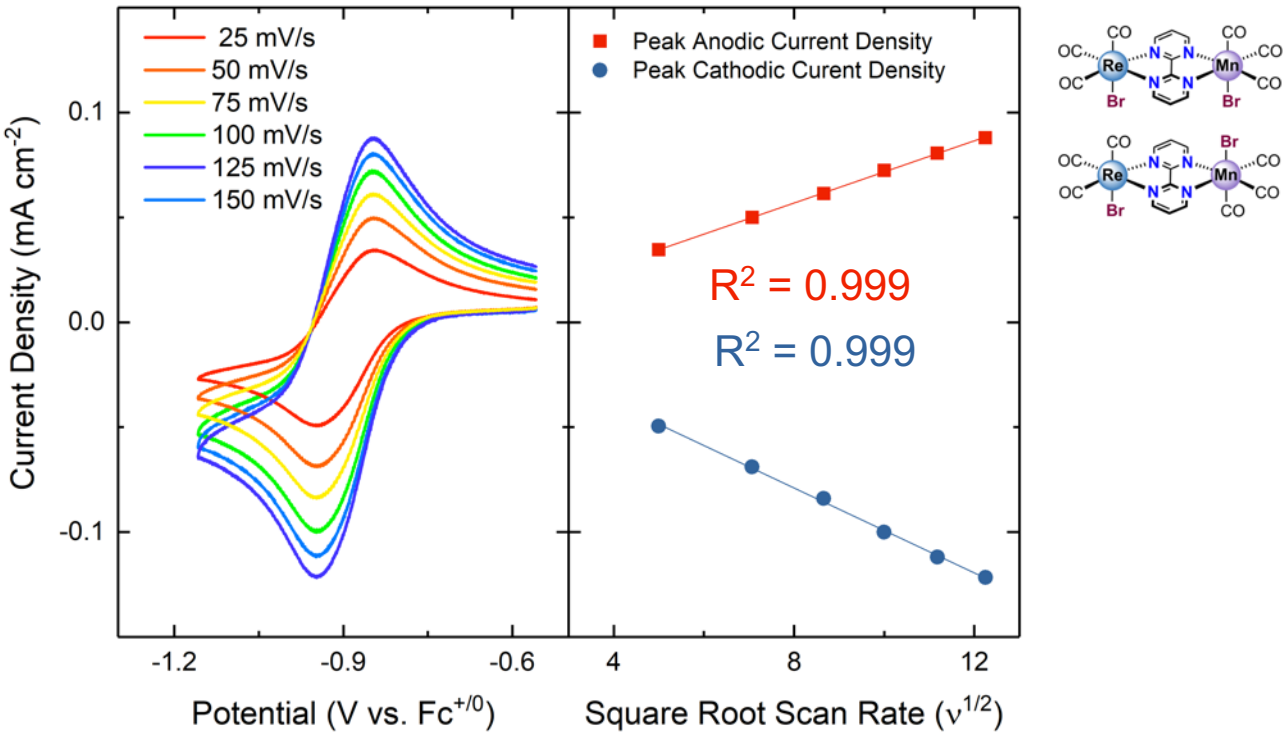

Figure S31: Scan rate dependence studies (left) and peak anodic and cathodic current density as a function of the square root of scan rate (right) for complex **6-syn** + **6-anti**.

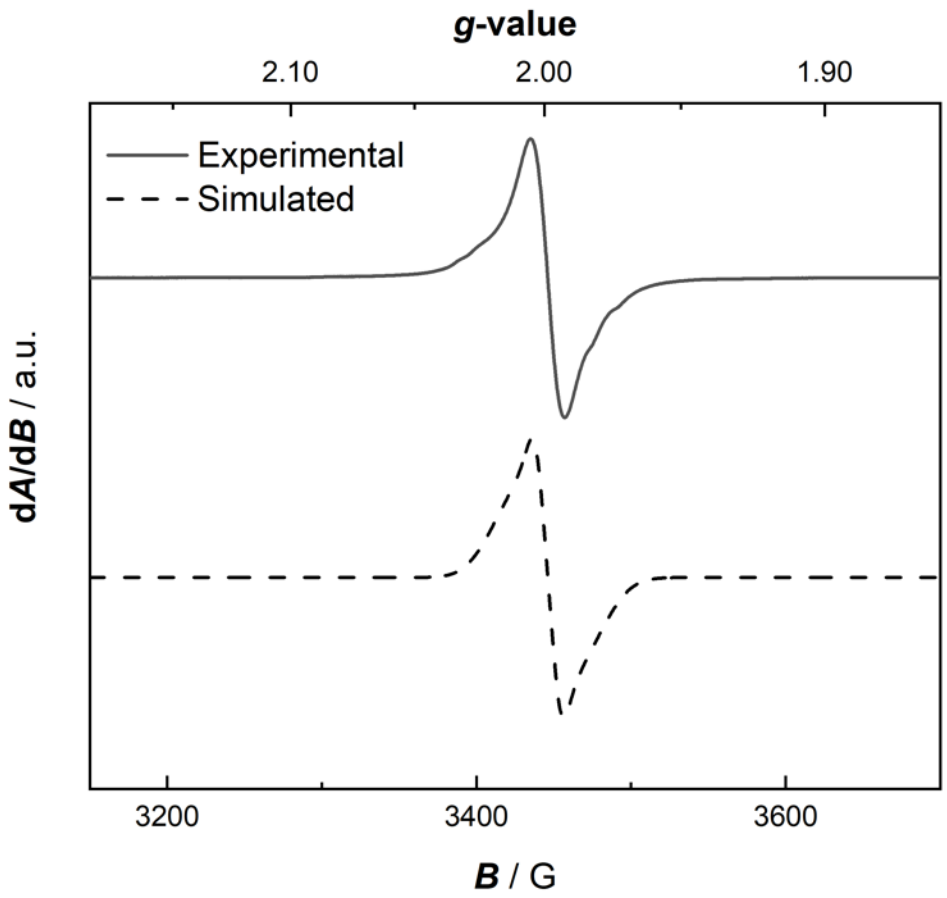

Figure S32: Experimental: perpendicular-mode X-band EPR spectrum of **2-syn** + **2-anti** after reduction by one e^- using Cp_2Co to generate a singly reduced paramagnetic species *in situ* (toluene, Temperature = 20 K, Frequency = 9.6405 GHz, Power = 2 mW). Simulated: Easyspin simulation of EPR data; Best values: g_x = 1.99, g_y = 2.01, g_z = 1.98, A_x = 43 MHz, A_y = 50 MHz, A_z = 15 MHz, HStrain(x) = 1 MHz, HStrain(y) = 100 MHz, HStrain(z) = 100 MHz, peak to peak line width (lwpp) = 0.75, weight = 1.

Crystallographic Information

Refinement Details

X-ray Crystallographic Studies for 1, 2-anti, 3, 4, 5-syn, 5-anti, and 6-syn

Crystals were mounted on polyimide MiTeGen loops with STP Oil Treatment and placed under a nitrogen stream. Low temperature (100 K) X-ray data were collected on a Bruker AXS D8 KAPPA diffractometer with an APEX II CCD detector and TRIUMPH graphite monochromator running at 50 kV and 30 mA with Mo radiation (K_α = 0.71073 Å) for **1** and on a Bruker AXS D8 VENTURE KAPPA diffractometer with PHOTON 100 CMOS detector and Helios focusing multilayer mirror optics running at 50 kV and 1 mA using Cu radiation (K_α = 1.54178 Å) for **5-syn** and **5-anti** and using Mo radiation (K_α = 0.71073 Å) for **2-anti**, **3**, **4**, and **6-syn.** Totals of 2374 (**1**), 2053 (**2-anti**), 2444 (**3**), 1206 (**4**), 1338 (**5-syn**), 2013 (**5-anti**), 884 (**6-syn**), 0.5° or 1.0° -wide ω- *or* ϕ-scan frames were collected with counting times of 10-20 seconds (**1**), 4-30 seconds (**2**), 1-10 seconds (**3**), 1-20 seconds (**4**), 5-60 seconds (**5-syn**), 1-15 seconds (**5-anti**), and 2-60 seconds (**6-syn**). Preliminary lattice constants were obtained with the Bruker Apex2 Software Suite.[1] Integrated reflection intensities for all compounds were produced using SAINT in the Bruker Apex2 Software Suite. Each data set was corrected empirically for variable absorption effects with SADABS[2] using equivalent reflections. The Bruker software package SHELXTL was used to solve each structure using intrinsic direct methods phasing. Final stages of weighted full-matrix least-squares refinement were conducted using F_o^2 data with SHELXTL[3] or the Olex2 software package equipped with XL[4]. All non-hydrogen atoms were refined anisotropically. All hydrogen atoms were included into the model at geometrically calculated positions and refined using a riding model. The isotropic displacement parameters of all hydrogen atoms were fixed to 1.2 times the *U* value of the atoms they are linked to. The relevant crystallographic and structure refinement data for all seven structures are given in Table S1.

Table S1: Crystal Refinement Data

	1 (a15100)	**2-anti** (p15249)	**3** (p15315)
CCDC accession code	2005316	2005317	2005320
Empirical formula	$C_{11}H_6ClN_4O_3Re$	$C_{14}H_6Cl_2N_4O_6Re_2$	$C_{11}H_6BrMnN_4O_3$
Formula weight	463.85	769.53	377.05
Temperature	100 K	100 K	100 K
Wavelength	0.71073 Å	0.71073 Å	0.71073 Å
Crystal system	monoclinic	monoclinic	triclinic
Space group	$P2_1/c$ (No. 14)	$P2_1/c$ (No. 14)	$P\text{-}1$ (No. 2)
a	6.2872(3) Å	6.3386(3) Å	6.6093(3) Å
b	14.9679(7) Å	11.9351(6) Å	6.6618(3) Å
c	13.4775(7) Å	12.3347(6) Å	14.8504(8) Å
α	90°	90°	102.3575(17)°
β	102.408(2)°	97.6407(17)°	93.1195(18)°
γ	90°	90°	102.3828(17)°
Volume	1238.69(11) $Å^3$	924.86(8) $Å^3$	620.40(5) $Å^3$
Z	4	2	2
Density (calculated)	2.487 g/cm^3	2.763 g/cm^3	2.018 g/cm^3
Absorption coefficient	10.038 mm^{-1}	13.406 mm^{-1}	4.296 mm^{-1}
F(000)	864	700	368
Crystal size	0.4 x 0.06 x 0.02 mm^3	0.06 x 0.04 x 0.02 mm^3	0.300 x 0.150 x 0.100 mm^3
Number of data frames/time	2374/10-20 seconds	2053/4-30 seconds	2444/1-10 seconds
Theta range	2.06 to 29.992°	2.385 to 24.992°	3.173 to 36.362°
Index ranges	$-8\le h\le 8$, $-21\le k\le 21$, $-18\le l\le 18$	$-7\le h\le 7$, $-14\le k\le 14$, $-14\le l\le 14$	$-10\le h\le 10$, $-10\le k\le 11$, $-24\le l\le 24$
Reflections collected	32945	21581	31855
Independent reflections	3602 [R_{int} = 0.039]	1634 [R_{int} = 0.055]	5964 [R_{int} = 0.038]
Completeness/θ_{max}	100%/25.000°	100%/24.992°	99.9%/25.242°
Absorption correction	Multi-scan	Multi-scan	Mulit-scan
Max. and min. transmission	1.000 and 0.630	1.000 and 0.852	0.7471 and 0.5920
Refinement method	Full-matrix least-squares on F^2	Full-matrix least-squares on F^2	Full-matrix least-squares on F^2
Data / restraints / parameters	3602 / 0 / 193	1634 / 0 / 145	5964 / 0 / 181
Goodness-of-fit on F^2	1.252	1.401	1.040
Final R indices [I>2σ(I)]	R_1 = 0.0212, wR_2 = 0.0453	R_1 =0.0267, wR_2 = 0.0478	R_1 =0.0289, wR_2 = 0.0572
R indices (all data)	R_1 = 0.0226, wR_2 = 0.0457	R_1 = 0.0304, wR_2 = 0.0485	R_1 = 0.0411, wR_2 = 0.0605
Largest diff. peak and hole	1.19 and -0.91 $e^-/Å^3$	1.57 and -1.79 $e^-/Å^3$	0.778 and -0.778 $e^-/Å^3$

	4 (p15260)	**5-syn** (p15288)	**5-anti** (p15287)
CCDC accession code	2005318	2005315	2005321
Empirical formula	$C_{11}H_6BrMnN_4O_3$	$C_{17}H_{12}Br_2Mn_2N_4O_7$	$C_{14}H_6Br_2Mn_2N_4O_6$
Formula weight	377.05	647.96	595.93
Temperature	100 K	100 K	100 K
Wavelength	0.71073 Å	1.54178 Å	1.54178 Å
Crystal system	monoclinic	orthorhombic	triclinic
Space group	*$P2_1/c$* (No. 14)	*Cmcm* (No. 63)	*P-1* (No. 2)
a	6.4216(2) Å	17.597(3) Å	6.4380(6) Å
b	14.7565(6) Å	10.830(2) Å	8.3336(7) Å
c	13.5124(5) Å	11.8313(18) Å	9.4980(9) Å
α	90°	90°	98.880(7)°
β	102.0331(12)°	90°	100.604(7)°
γ	90°	90°	96.117(7)°
Volume	1252.30(8) $Å^3$	2254.8(7) $Å^3$	490.08(8) $Å^3$
Z	4	4	1
Density (calculated)	2.000 g/cm^3	1.909 g/cm^3	2.019 g/cm^3
Absorption coefficient	4.257 mm^{-1}	13.687 mm^{-1}	15.626 mm^{-1}
F(000)	736	1248.0	286
Crystal size	0.250 x 0.100 x 0.050 mm^3	0.1 x 0.03 x 0.03 mm^3	0.070 x 0.050 x 0.030 mm^3
Number of data frames/time	1206/1-20 seconds	1338/5-60 seconds	2013/1-15 seconds
Theta range	3.083 to 36.307°	4.794 to 74.214°	4.814 to 72.057°
Index ranges	$-10\leq h\leq 10$, $-24\leq k\leq 24$, $-22\leq l\leq 22$	$-21\leq h\leq 19$, $-13\leq k\leq 11$, $-14\leq l\leq 9$	$-6\leq h\leq 7$, $-10\leq k\leq 10$, $-11\leq l\leq 11$
Reflections collected	28709	4267	5479
Independent reflections	6048 [R_{int} = 0.039]	1178[R_{int} = 0.109]	1911[R_{int} = 0.092]
Completeness/θ_{max}	99.9%/25.242°	97.9%/66.00°	99.7%/67.679°
Absorption correction	Multi-scan	None	Multi-scan
Max. and min. transmission	0.7474 and 0.5901	0.7538 and 0.5415	0.7538 and 0.5580
Refinement method	Full-matrix least-squares on F^2	Full-matrix least-squares on F^2	Full-matrix least-squares on F^2
Data / restraints / parameters	6048 / 0 / 181	1178 / 29 / 93	1911 / 0 / 127
Goodness-of-fit on F^2	1.045	1.065	1.062
Final R indices [I>2σ(I)]	R_1 =0.0309, wR_2 = 0.0638	R_1 = 0.0616, wR_2 = 0.1333	R_1 = 0.0702, wR_2 = 0.1569
R indices (all data)	R_1 =0.0476, wR_2 = 0.0687	R_1 = 0.1106, wR_2 = 0.1538	R_1 = 0.1034 wR_2 = 0.1759
Largest diff. peak and hole	0.969 and -0.693 $e^-/Å^3$	0.97 and -1.13 $e^-/Å^3$	1.451 and -0.966 $e^-/Å^3$

	6-syn (p15317)
CCDC accession code	2005319
Empirical formula	$C_{17}H_{12}Br_2MnN_4O_7Re$
Formula weight	785.27
Temperature	100 K
Wavelength	0.71073 Å
Crystal system	orthorhombic
Space group	*Cmcm* (No 63)
a	17.6165(8) Å
b	10.9052(5) Å
c	11.8240(6) Å
α	90°
β	90°
γ	90°
Volume	2271.53(19) $Å^3$
Z	4
Density (calculated)	2.296 g/cm^3
Absorption coefficient	9.444 mm^{-1}
F(000)	1472
Crystal size	0.100 x 0.030 x 0.030 mm^3
Number of data frames/time	884/2-60 seconds
Theta range	2.196 to 30.501°
Index ranges	$-22\leq h\leq 25$, $-14\leq k\leq 14$, $-16\leq l\leq 15$
Reflections collected	15274
Independent reflections	1811[R_{int} = 0.056]
Completeness/θ_{max}	99.9%/25.242°
Absorption correction	Multi-scan
Max. and min. transmission	0.7466 and 0.5762
Refinement method	Full-matrix least-squares on F^2
Data / restraints / parameters	1811 / 199 / 126
Goodness-of-fit on F^2	1.060
Final R indices [I>2σ(I)]	R_1 = 0.0286, wR_2 = 0.0489
R indices (all data)	R_1 = 0.0448, wR_2 = 0.0519
Largest diff. peak and hole	0.892 and -1.442 $e^-/Å^3$

Special Refinement Details for 1.

Complex **1** crystalizes in the monoclinic space group $P2_1/c$. The crystal exhibits disorder in regard to the axial CO and axial Cl. Specifically, the disorder was modeled by refining the relative occupancies of Cl1 and Cl1a, giving a ratio of 94:6. Additionally, refinement of the relative occupancies of O3 and O3a revealed a ratio of 94:6.

Solid-State Structure of Complex 1.

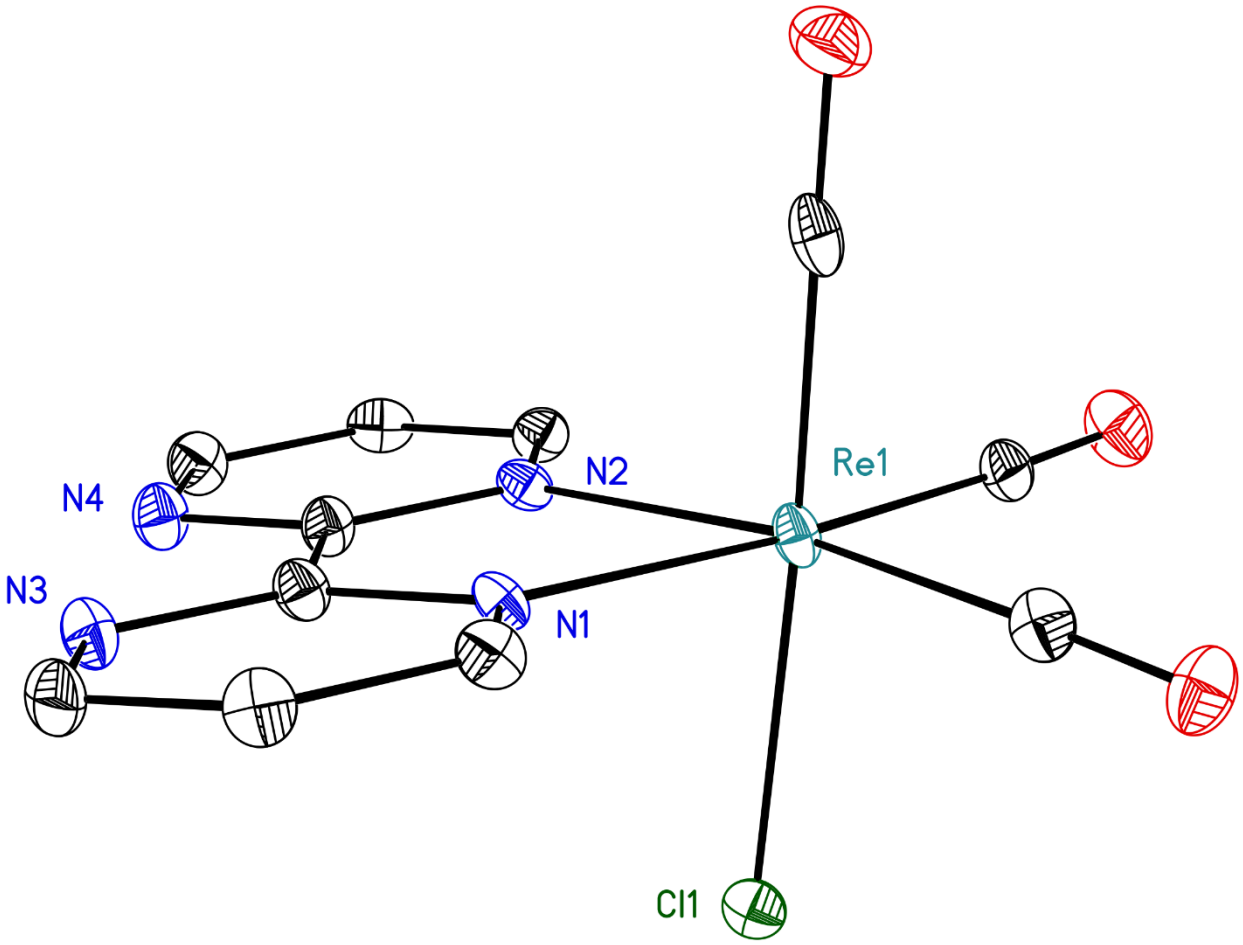

Figure S33. Solid-state structure of complex **1**. Partial occupancy CO and Cl omitted for clarity. Hydrogen atoms are omitted for clarity. Displacement ellipsoids are shown at the 50% probability level.

Full Solid-state Structure of Complex 1.

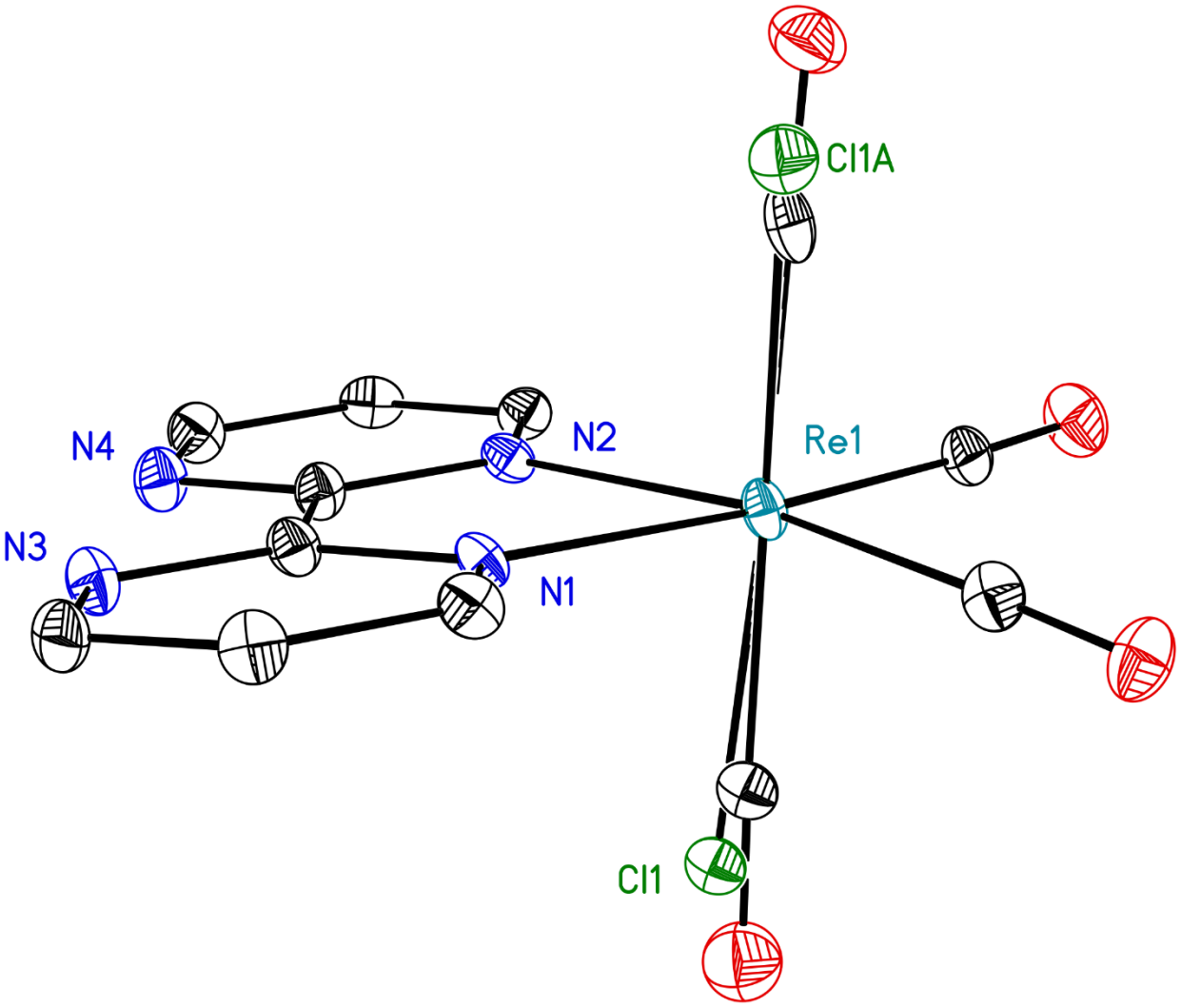

Figure S34. Full solid-state structure of complex **1**. Hydrogen atoms are omitted for clarity. Displacement ellipsoids are shown at the 50% probability level.

Special Refinement Details for 2-anti.

Complex **2-anti** crystalizes in the monoclinic space group *$P2_1/C$*. The crystal exhibits disorder in regard to the axial CO and axial Cl ligands. Specifically, the disorder was modeled by refining the relative occupancies of Cl1 and Cl1A, giving a ratio of 80:20. Additionally, refinement of the relative occupancies of C7 and C7A, as well as O3 and O3A, revealed a ratio of 80:20.

Solid-State Structure of Complex 2-anti.

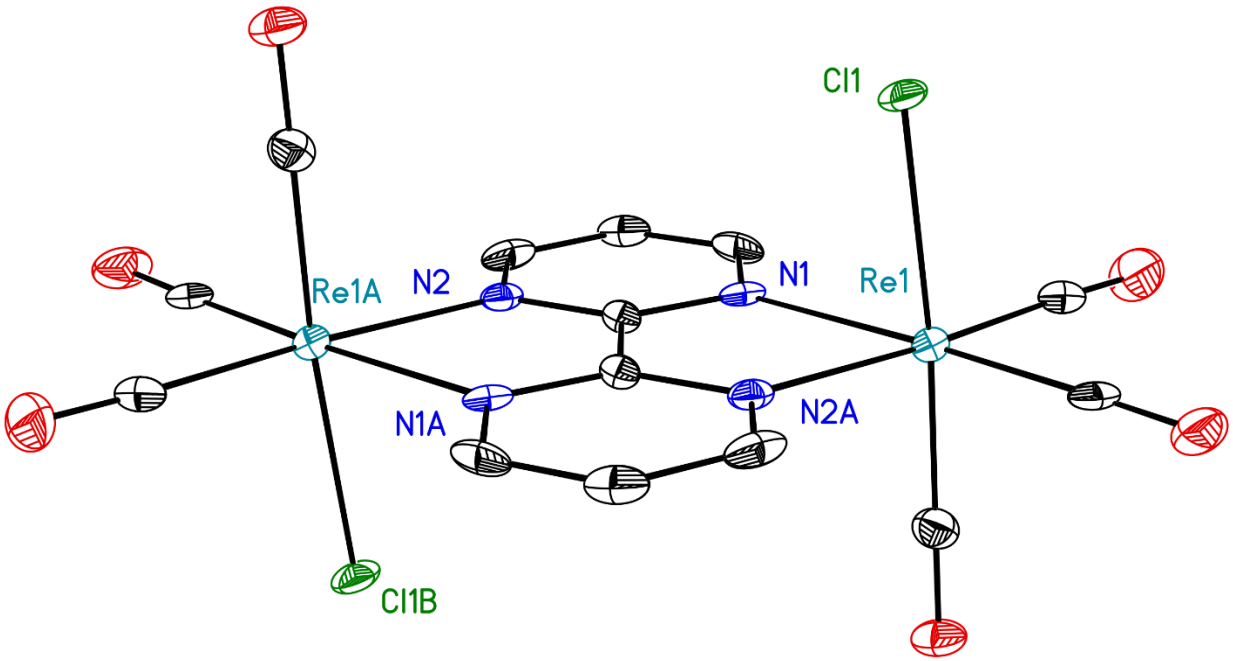

Figure S35: Solid-state structure of complex **2-anti**. Partial occupancy Cl1A, Cl1C, C7A, O3A, C7AA, and O3AA atoms are omitted for clarity. Hydrogen atoms are omitted for clarity. Displacement ellipsoids are shown at the 50% probability level.

Full Solid-State Structure of Complex 2-anti.

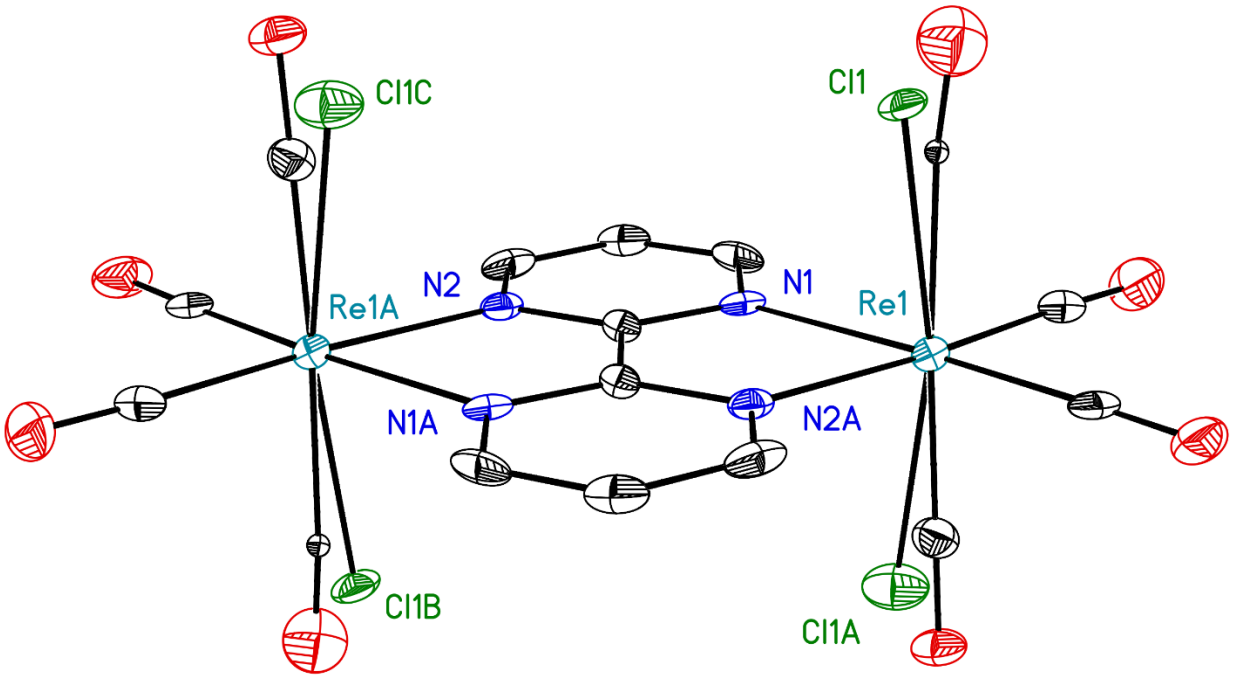

Figure S36: Full solid-state structure of complex **2-anti**, showing admixture of **2-syn** that is also present in the unit cell due to packing disorder. Hydrogen atoms are omitted for clarity. Displacement ellipsoids are shown at the 50% probability level.

Special Refinement Details for 3.

No special refinement was required.

Full Solid-State Structure of Complex 3.

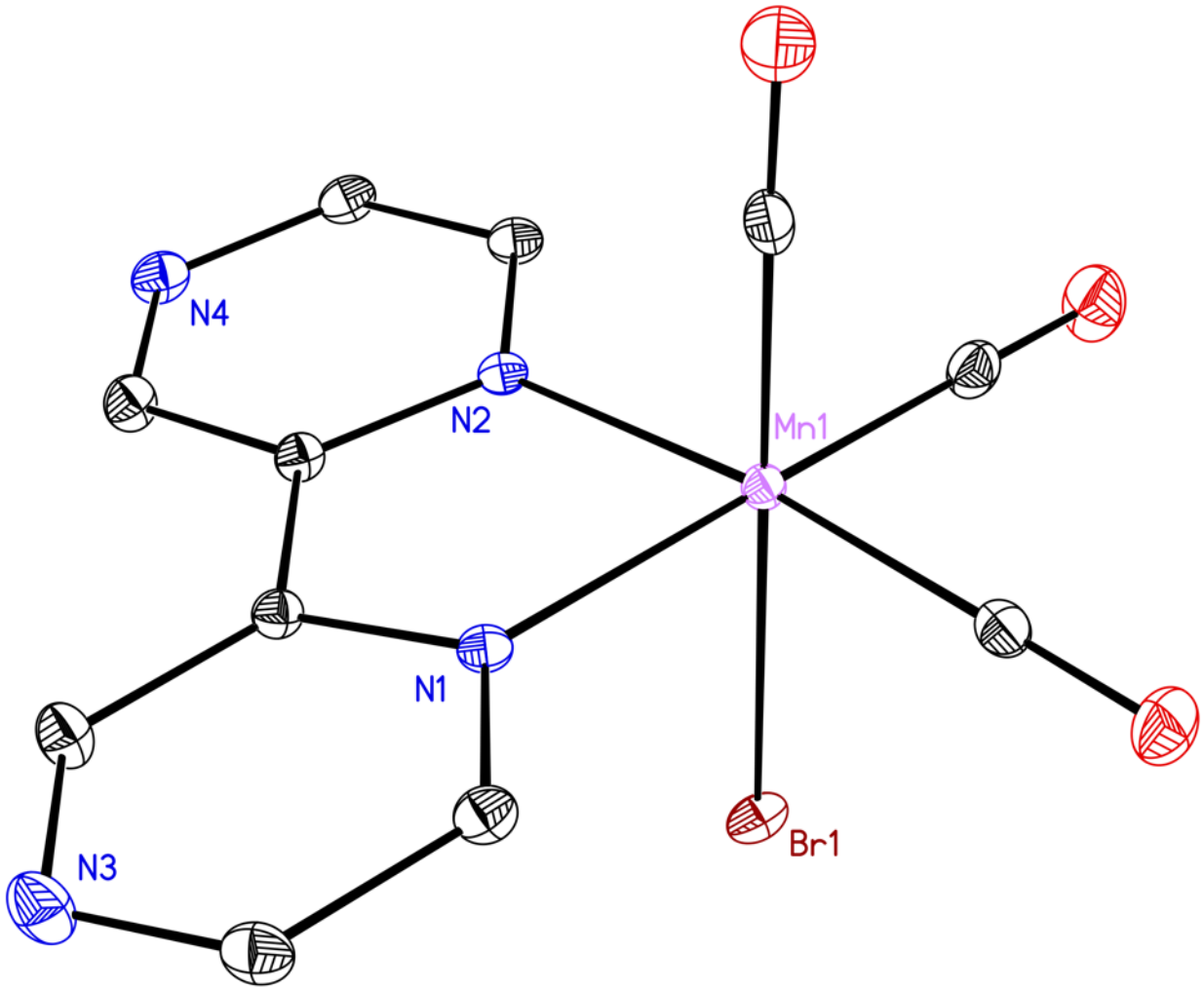

Figure S37. Full solid-state structure of complex **3**. Hydrogen atoms are omitted for clarity. Displacement ellipsoids are shown at the 50% probability level.

Special Refinement Details for 4.

Complex **4** crystallizes in the monoclinic space group $P2_1/c$ with one molecule in the asymmetric unit. The highest electron density maximum is located in a position consistent with a bromine disordered with carbon monoxide (C1 and O11). This disorder was not modeled because the occupancy of this bromine refined to less than 5% and no partially occupied carbon monoxide could be located in the bromine position (Br1).

Full Solid-State Structure of Complex 4.

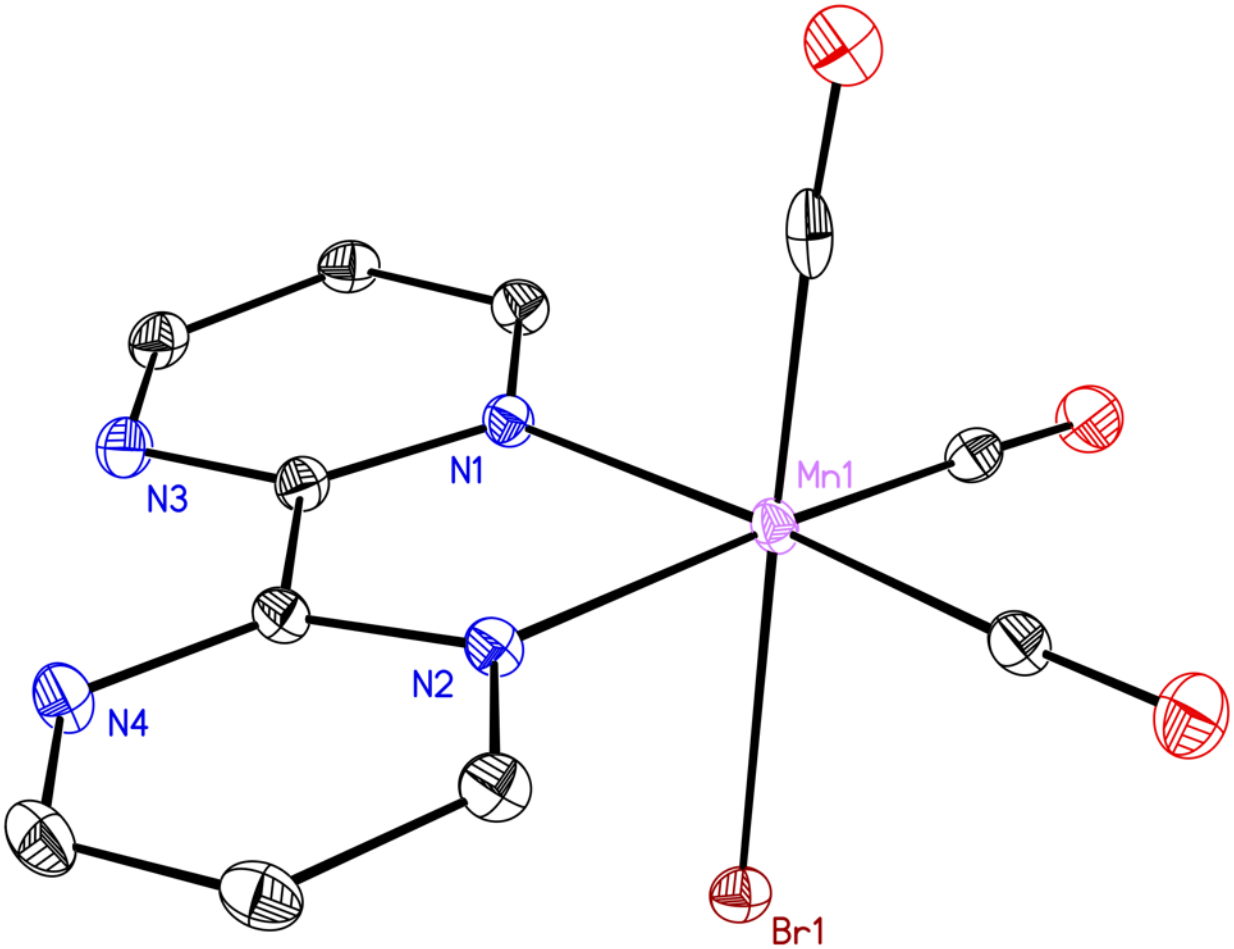

Figure S38: Full solid-state structure of complex **4**. Hydrogen atoms are omitted for clarity. Displacement ellipsoids are shown at the 50% probability level.

Special Refinement Details for 5-syn.

Complex **5-syn** crystallizes in the orthorhombic space group *Cmcm* with one quarter of a molecule in the asymmetric unit along with a quarter of an acetone. The occupancy of the acetone molecule was decreased to a quarter because it is located on multiple symmetry elements (mirrors and two-fold rotation axis). The acetone was refined with the help of similarity restraints on the 1,2- and 1,3-distances and displacement parameters as well as rigid bond restraints for anisotropic displacement parameters. In addition, the C-C distances were restrained to be 1.51(4) Å and all atoms were restrained to be flat. The quality of this crystal is relatively poor because is appeared to decompose over the course of data collection, possibly due to light exposure.

Solid-State Structure of Complex 5-syn.

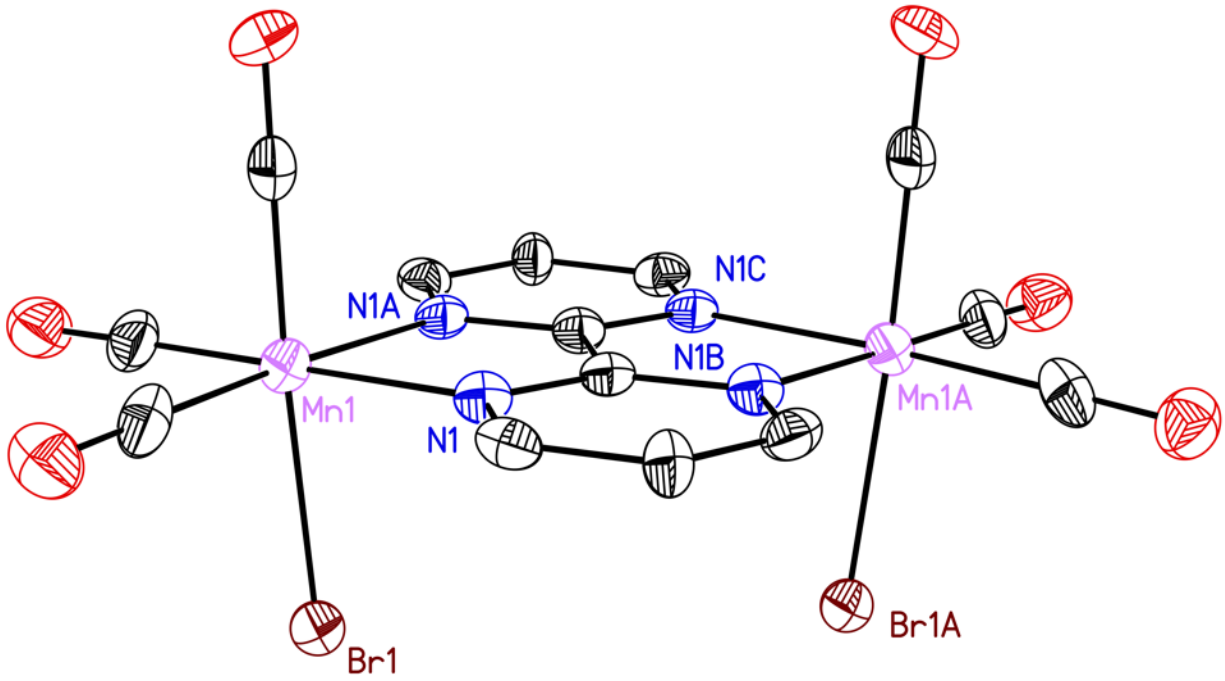

Figure S39: Solid-state structure of complex **5-syn**. Hydrogen atoms and a disordered acetone molecule are omitted for clarity. Displacement ellipsoids are shown at the 50% probability level.

Full Solid-State Structure of Complex 5-syn.

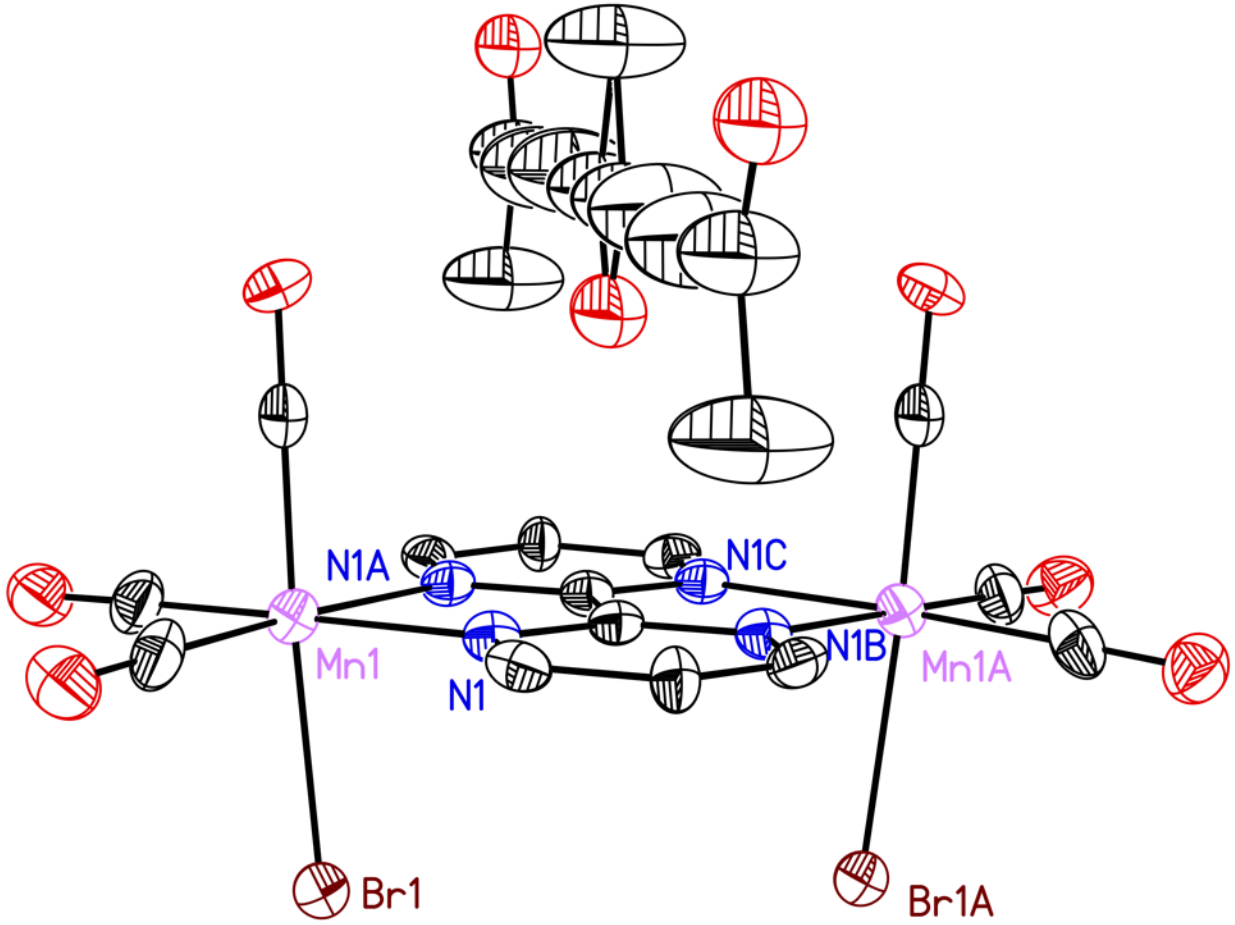

Figure S40: Solid-state structure of complex **5-syn**. Hydrogen are omitted for clarity. Displacement ellipsoids are shown at the 50% probability level.

Special Refinement Details for 5-anti.

No special refinement was required.

Full Solid-State Structure of Complex 5-anti.

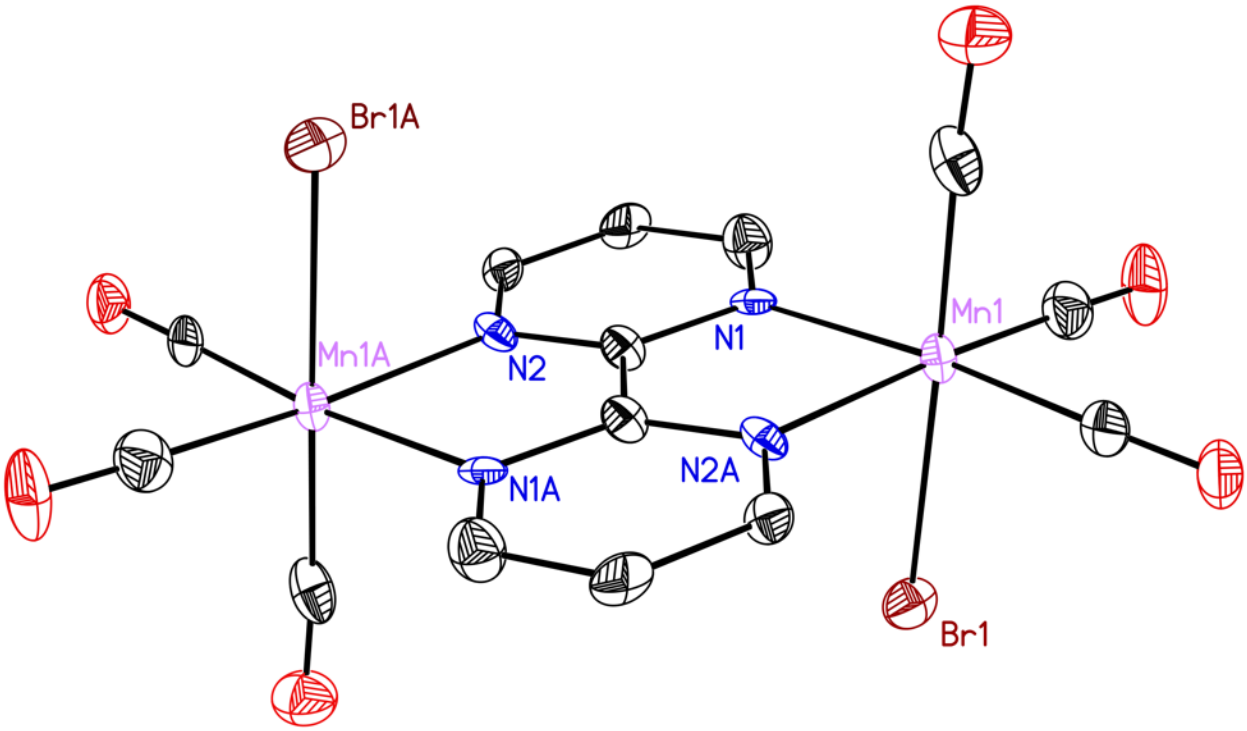

Figure 41: Full solid-state structure of **5-anti.** Hydrogen are omitted for clarity. Displacement ellipsoids are shown at the 50% probability level.

Special Refinement Details for 6-syn.

Compound **6-syn** crystallizes in the orthorhombic space group *Cmcm* with a quarter of a molecule in the asymmetric unit along with a quarter of an acetone. All disordered atoms were refined with the help of similarity restraints on the 1,2- and 1,3-distances and displacement parameters as well as rigid or enhanced rigid bond restraints for anisotropic displacement parameters. The molecule is located on multiple symmetry elements (mirror planes and a 2-fold rotation axis). Due to this situation, only one metal position is present in the asymmetric unit which was modeled as a mixture of Mn and Re. Refinement of the relative occupancies of Mn and Re gave a ratio of approximately 49.4:50.6. For the final refinement the occupancies of Mn and Re were constrained to be 50:50 and the anisotropic displacement parameters were constrained to be equal. As a result of the Mn-Re disorder, the carbonyl ligands were also disordered.

The occupancy of the acetone molecule was decreased to a quarter because it is located on multiple symmetry elements (mirror planes and two-fold rotation axis). The acetone was refined with the help of similarity restraints on the 1,2- and 1,3-distances and displacement parameters as well as rigid bond restraints for anisotropic displacement parameters. In addition, the C-C distances were restrained to be 1.51(4) Å and all atoms were restrained to be flat.

Solid-State Structure of Complex 6-syn.

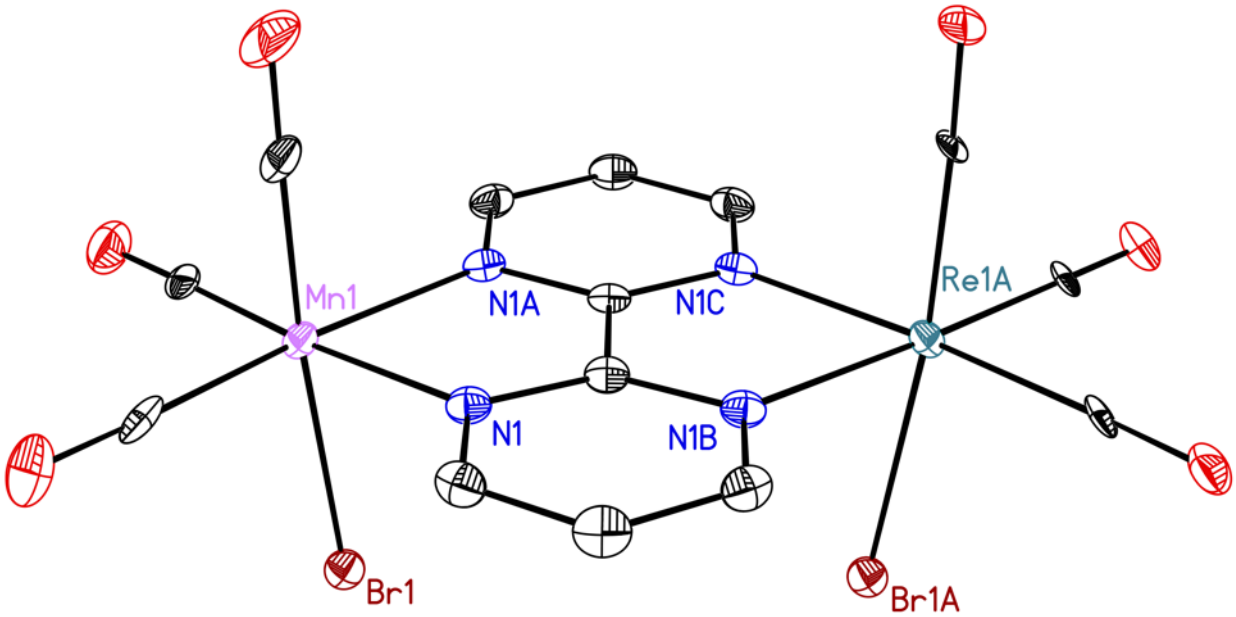

Figure S42: Solid-state structure of complex **6-syn**. Hydrogen atoms, a disordered acetone molecule, and a disordered molecule of **6-syn** are omitted for clarity. Displacement ellipsoids are shown at the 50% probability level.

Full Solid-State Structure of Complex 6-syn.

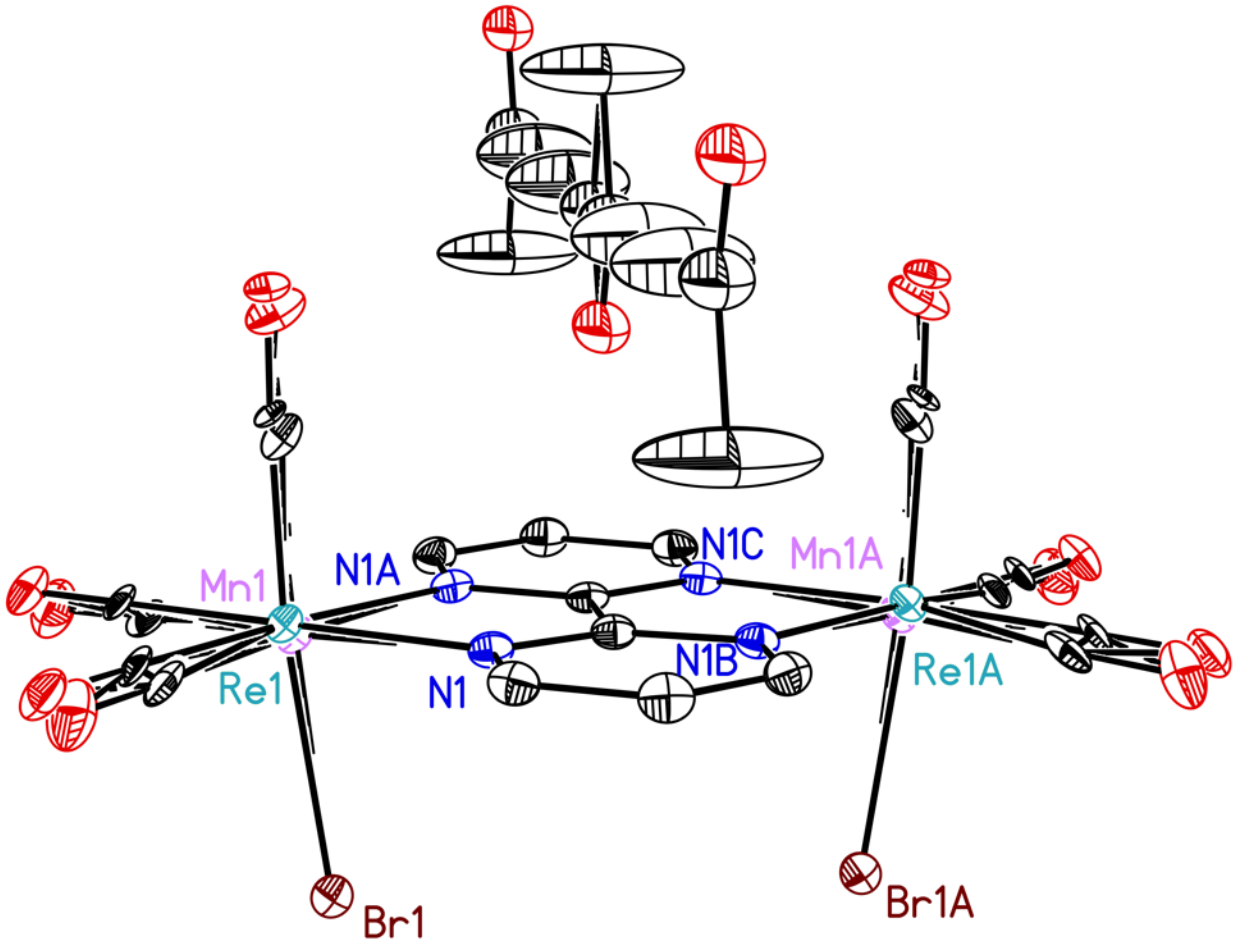

Figure S43: Solid-state structure of complex **6-syn**. Hydrogen atoms are omitted for clarity. Displacement ellipsoids are shown at the 50% probability level.

References

[1] APEX2, Version 2 User Manual, M86-E01078, Bruker Analytical X-ray Systems: Madison, WI, June 2006.

[2] G. M. Sheldrick, SADABS (version 2008/1): Program for Absorption Correction for Data from Area Detector Frames, University of Göttingen, 2008.

[3] G. M. Sheldrick, Crystal structure refinement with SHELXL. *Acta Crystallogr., Sect. A: Found. Crystallogr.* 2015, **71**, 3-8.

[4] O. V. Dolomanov, L. J. Bourhis, R. J. Gildea, J. A. K. Howard, H. J. Puschmann, *Appl. Crystallogr.* 2009, **42**, 339-341.